

**EFFECT OF POROUS MEDIUM AND MAGNETIC FIELD ON ENTROPY
GENERATION OF AN INCOMPRESSIBLE FLOW IN AN INCLINED
CHANNEL**

**M.Sc. Thesis by
Murat HAVZALI**

Department : Faculty of Aeronautics and Astronautics

Programme : Interdisciplinary M.Sc.

JANUARY 2010

**EFFECT OF POROUS MEDIUM AND MAGNETIC FIELD ON ENTROPY
GENERATION OF AN INCOMPRESSIBLE FLOW IN AN INCLINED
CHANNEL**

**M.Sc. Thesis by
Murat HAVZALI
511071122**

**Date of submission : 25 December 2009
Date of defence examination: 27 January 2010**

**Supervisor (Chairman) : Assis. Prof. Dr. H. İbrahim KESER (ITU)
Members of the Examining Committee : Prof. Dr. İbrahim ÖZKOL (ITU)
Assis. Prof. Dr. Güven KÖMÜRGÖZ (ITU)**

JANUARY 2010

İSTANBUL TEKNİK ÜNİVERSİTESİ ★ FEN BİLİMLERİ ENSTİTÜSÜ

**EĞİK KANALDA SIKIŞTIRILAMAZ AKIŞTA GÖZENEKLİ ORTAM VE
MANYETİK ALAN ŞARTLARININ ENTROPİ ÜRETİMİNE ETKİSİ**

**YÜKSEK LİSANS TEZİ
Murat HAVZALI
511071122**

**Tezin Enstitüye Verildiği Tarih : 25 Aralık 2009
Tezin Savunulduğu Tarih : 27 Ocak 2010**

**Tez Danışmanı : Yard. Doç. Dr. H. İbrahim KESER (İTÜ)
Diğer Jüri Üyeleri : Prof. Dr. İbrahim ÖZKOL (İTÜ)
Yard. Doç. Dr. Güven KÖMÜRGÖZ (İTÜ)**

OCAK 2010

FOREWORD

I would like to express my deep appreciation and thanks for my advisor, Assis. Prof. Dr. Mr. Hacı İbrahim Keser, Assis. Prof. Dr. Mrs. Güven Kömürgöz, Prof. Dr. Mr. İbrahim Özkol for their time and interest in this thesis; and my loving family for their never-ending love, support and belief.

JANUARY 2010

Murat Havzalı

Astronautical Engineer

TABLE OF CONTENTS

	<u>Page</u>
FOREWORD	v
TABLE OF CONTENTS	vii
LIST OF TABLES	ix
LIST OF FIGURES	xi
LIST OF SYMBOLS	xv
SUMMARY	xvii
ÖZET	xix
1. INTRODUCTION	1
1.1 Purpose Of The Thesis	4
2. THEORY	5
2.1 Non-dimensionalizations and Dimensionless Parameters	5
2.1.1 Peclet Number	6
2.1.2 Brinkman Number	6
2.1.3 Darcy Number	6
2.1.4 Hartmann Number	7
2.2 Continuity Equation	7
2.3 Momentum Equation	8
2.3.1 Clear channel	11
2.3.2 Presence of porous medium	12
2.3.3 Presence of magnetic field	13
2.3.4 Presence of both porous medium and magnetic field	14
2.4 Energy Equation	15
2.4.1 Clear channel	17
2.4.2 Presence of porous medium	17
2.4.3 Presence of magnetic field	17
2.4.4 Presence of both porous medium and magnetic field	18
2.5 Entropy Generation	18
2.5.1 Entropy generation number	21
2.5.2 Bejan number	21
2.5.3 Clear channel	22
2.5.4 Presence of porous medium	22
2.5.5 Presence of magnetic field	23
2.5.6 Presence of both porous medium and magnetic field	23
2.6 Solution Methods	24
2.6.1 Some analytic solutions	24
2.6.2 The core numerical scheme	25
2.6.2.1 Stability of the core scheme	26
2.6.2.2 Consistency of the core scheme	27
3. RESULTS AND DISCUSSION	29
3.1 Clear Channel	30
3.1.1 Dirichlet problem	30

3.1.2 Neumann problem	33
3.2 Presence of Porous Medium	34
3.2.1 Dirichlet problem	35
3.2.2 Neumann problem	36
3.3 Presence of Magnetic Field	38
3.3.1 Dirichlet problem	38
3.3.2 Neumann problem	40
3.4 Presence of both Porous Medium and Magnetic Field.....	42
3.4.1 Dirichlet problem	42
3.4.2 Neumann problem	52
4. CONCLUSION AND RECOMENDATIONS	63
REFERENCES	65
CURRICULUM VITA.....	69

LIST OF TABLES

	<u>Page</u>
Table 2.1: Inlet and outlet of a differential control volume	7
Table 3.1: Error comparison between NDSolve and the core code for Dirichlet problems.....	30

LIST OF FIGURES

	<u>Page</u>
Figure 2.1 : Differential control volume and mass inlet-outlet in x direction	7
Figure 2.2 : Geometry of clear channel case.....	11
Figure 2.3 : Geometry of the porous case	12
Figure 2.4 : Geometry of the magnetic field case	13
Figure 2.5 : Geometry for both porous and magnetic case	14
Figure 2.6 : Local entropy generation by convection heat transfer	19
Figure 3.1 : The error dependance on grid size.....	29
Figure 3.2 : Velocity profile of clear channel	31
Figure 3.3 : Temperature profile of clear channel for different \bar{x} stations at $Br = 0.1$	31
Figure 3.4 : Entropy generation at different \bar{x} stations at $\bar{x} = 0.2$, $Pe = 100$, $Br\Omega^{-1} = 0.1$	32
Figure 3.5 : Bejan number at different \bar{x} station at $Pe = 100$, $Br\Omega^{-1} = 0.1$	32
Figure 3.6 : Temperature profile of clear channel for different \bar{x} stations at $Br = 0.1$	33
Figure 3.7 : Entropy generation for different \bar{x} profiles at $Pe = 100$, $Br\Omega^{-1} = 0.1$	34
Figure 3.8 : Bejan number for different \bar{x} stations at $Pe = 100$, $Br\Omega^{-1} = 0.1$	34
Figure 3.9 : Velocity profiles of the porous case for different Da	35
Figure 3.10 : Temperature profiles for different \bar{x} stations at $Br = 0.1$, $Da = 0.1$	35
Figure 3.11 : Entropy generation for different \bar{x} stations at $Pe = 100$, $Br\Omega^{-1} = 0.1$, $Da = 0.1$	36
Figure 3.12 : Bejan number for different \bar{x} stations at $Pe = 100$, $Br\Omega^{-1} = 0.1$, $Da = 0.1$	36
Figure 3.13 : Temperature profiles for different \bar{x} stations at $Br = 0.1$, $Da = 0.1$	37
Figure 3.14 : Entropy generation for different \bar{x} stations at $Pe = 100$, $Br\Omega^{-1} = 0.1$, $Da = 0.1$	37
Figure 3.15 : Bejan number for different \bar{x} stations at $Pe = 100$, $Br\Omega^{-1} = 0.1$, $Da = 0.1$	38
Figure 3.16 : Velocity profiles of the magnetic case at different Ha	39
Figure 3.17 : Temperature profiles for different \bar{x} stations at $Br = 0.1$, $Ha = 3$	39
Figure 3.18 : Entropy generation for different \bar{x} stations at $Pe = 100$, $Br\Omega^{-1} = 0.1$, $Ha = 3$	40
Figure 3.19 : Bejan number for different \bar{x} stations at $Pe = 100$, $Br\Omega^{-1} = 0.1$, $Ha = 3$	40
Figure 3.20 : Temperature profiles for different \bar{x} stations at $Pe = 100$, $Br = 0.1$, $Ha = 3$	41
Figure 3.21 : Entropy generation for different \bar{x} stations at $Pe = 100$, $Br\Omega^{-1} = 0.1$, $Ha = 3$	41

Figure 3.22 : Bejan number for different \bar{x} stations at $Pe = 100$, $Br\Omega^{-1} = 0.1$, $Ha = 3$	42
Figure 3.23 : Comparison of analytical and numerical results of magnetic neumann case	42
Figure 3.24 : Velocity profile both porous and magnetic case for different Da at $Ha = 3$	43
Figure 3.25 : Velocity profile both porous and magnetic case for different Ha at $Da = 0.1$	43
Figure 3.26 : Temperature profiles for different \bar{x} stations at $Pe = 100$, $Br = 0.1$, $Da = 0.1$, $Ha = 3$	44
Figure 3.27 : Temperature profiles for different Br at $\bar{x} = 0.2$, $Pe = 100$, $Da = 0.1$, $Ha = 3$	44
Figure 3.28 : Temperature profiles for different Da at $Pe = 100$, $Br = 0.1$, $Ha = 3$	45
Figure 3.29 : Temperature profiles for different Ha at $Pe = 100$, $Br = 0.1$, $Da = 0.1$	45
Figure 3.30 : Entropy generation for different \bar{x} stations at $Pe = 100$, $Br\Omega^{-1} = 0.1$, $Da = 0.1$, $Ha = 3$	46
Figure 3.31 : Entropy generation for different Pe at $\bar{x} = 0.2$, $Br\Omega^{-1} = 0.1$, $Da = 0.1$, $Ha = 3$	46
Figure 3.32 : Entropy generation for different $Br\Omega^{-1}$ at $\bar{x} = 0.2$, $Pe = 100$, $Da = 0.1$, $Ha = 3$	47
Figure 3.33 : Entropy generation for different Da at $\bar{x} = 0.2$, $Pe = 100$, $Br\Omega^{-1} = 0.1$, $Ha = 3$	47
Figure 3.34 : Entropy generation for different Ha at $\bar{x} = 0.2$, $Pe = 100$, $Br\Omega^{-1} = 0.1$, $Da = 0.1$	48
Figure 3.35 : Bejan number for different \bar{x} stations at $Pe = 100$, $Br\Omega^{-1} = 0.1$, $Da = 0.1$, $Ha = 3$	48
Figure 3.36 : Bejan number for different Pe at $\bar{x} = 0.2$, $Br\Omega^{-1} = 0.1$, $Da = 0.1$, $Ha = 3$	49
Figure 3.37 : Bejan number for different $Br\Omega^{-1}$ at $\bar{x} = 0.2$, $Pe = 100$, $Da = 0.1$, $Ha = 3$	49
Figure 3.38 : Bejan number for different Da at $\bar{x} = 0.2$, $Pe = 100$, $Br\Omega^{-1} = 0.1$, $Ha = 3$	50
Figure 3.39 : Bejan number for different Ha at $\bar{x} = 0.2$, $Pe = 100$, $Br\Omega^{-1} = 0.1$, $Da = 0.1$	51
Figure 3.40 : Parts of entropy generation at $\bar{x} = 0.2$, $Pe = 100$, $Br\Omega^{-1} = 0.1$, $Da = 0.1$, $Ha = 3$	51
Figure 3.41 : Effect of viscous dissipation on temperature profiles at $Pe = 100$, $Br = 0.1$, $Da = 0.1$, $Ha = 3$	52
Figure 3.42 : Effect of viscous dissipation on entropy generation at $Pe = 100$, $Br\Omega^{-1} = 0.1$, $Da = 0.1$, $Ha = 3$	52
Figure 3.43 : Temperature profiles for different \bar{x} stations at $Pe = 100$, $Br = 0.1$, $Da = 0.1$, $Ha = 3$	53
Figure 3.44 : Temperature profiles for different Br at $\bar{x} = 0.2$, $Pe = 100$, $Da = 0.1$, $Ha = 3$	53

Figure 3.45 : Temperature profiles for different Da at $Pe = 100$, $Br = 0.1$, $Ha = 3$	54
Figure 3.46 : Temperature profiles for different Ha at $Pe = 100$, $Br = 0.1$, $Da = 0.1$	54
Figure 3.47 : Entropy generation for different \bar{x} stations at $Pe = 100$, $Br\Omega^{-1} = 0.1$, $Da = 0.1$, $Ha = 3$	55
Figure 3.48 : Entropy generation for different Pe at $\bar{x} = 0.2$, $Br\Omega^{-1} = 0.1$, $Da = 0.1$, $Ha = 3$	55
Figure 3.49 : Entropy generation for different $Br\Omega^{-1}$ at $\bar{x} = 0.2$, $Pe = 100$, $Da = 0.1$, $Ha = 3$	56
Figure 3.50 : Entropy generation for different Da at $\bar{x} = 0.2$, $Pe = 100$, $Br\Omega^{-1} = 0.1$, $Ha = 3$	57
Figure 3.51 : Entropy generation for different Ha at $\bar{x} = 0.2$, $Pe = 100$, $Br\Omega^{-1} = 0.1$, $Da = 0.1$	57
Figure 3.52 : Bejan number for different \bar{x} stations at $Pe = 100$, $Br\Omega^{-1} = 0.1$, $Da = 0.1$, $Ha = 3$	58
Figure 3.53 : Bejan number for different Pe at $\bar{x} = 0.2$, $Br\Omega^{-1} = 0.1$, $Da = 0.1$, $Ha = 3$	59
Figure 3.54 : Bejan number for different $Br\Omega^{-1}$ at $\bar{x} = 0.2$, $Pe = 100$, $Da = 0.1$, $Ha = 3$	59
Figure 3.55 : Bejan number for different Da at $\bar{x} = 0.2$, $Pe = 100$, $Br\Omega^{-1} = 0.1$, $Ha = 3$	60
Figure 3.56 : Bejan number for different Ha at $\bar{x} = 0.2$, $Pe = 100$, $Br\Omega^{-1} = 0.1$, $Da = 0.1$	60
Figure 3.57 : Parts of entropy generation at $\bar{x} = 0.2$, $Pe = 100$, $Br\Omega^{-1} = 0.1$, $Da = 0.1$, $Ha = 3$	61
Figure 3.58 : Effect of viscous dissipation on temperature profiles at $Pe = 100$, $Br = 0.1$, $Da = 0.1$, $Ha = 3$	61
Figure 3.59 : Effect of viscous dissipation on entropy generation at $Pe = 100$, $Br\Omega^{-1} = 0.1$, $Da = 0.1$, $Ha = 3$	62

LIST OF SYMBOLS

B	: Magnetic induction [Wb / m^2]
c_p	: Specific heat [$J / kg \cdot K$]
g	: Acceleration due to gravity [m / s^2]
h	: Half width of channel [m]
k	: Thermal conductivity [$W / (m \cdot K)$]
K	: Permeability [m^2]
N_f	: Entropy generation number due to fluid friction
N_h	: Entropy generation number due to heat transfer
N_m	: Entropy generation number due to magnetic field
N_p	: Entropy generation number due to porosity
N_s	: Entropy generation number
N_x	: x component of N_h
N_y	: y component of N_h
q	: Wall heat flux [W / m^2]
s	: Entropy [W / K]
S_G	: Entropy generation for unit volume [$W / m^3 K$]
T	: Temperature [K]
\bar{T}	: Dimensionless temperature
T_0	: Reference temperature [K]
T_w	: Wall temperature [K]
ΔT	: Temperature difference = qh / k or $= T_w - T_0$ [K]
u	: x component of velocity [m / s]
\bar{u}	: Dimensionless velocity = u / u_{av} or u / u_{\max}
u_{av}	: Average velocity [m / s]
u_{\max}	: Maximum velocity = $u_{@y=0}$ [m / s]
v	: y component of velocity
\vec{V}	: Velocity vector
w	: z component of velocity
x	: Axial distance [m]
\bar{x}	: Dimensionless axial distance
y	: Normal distance [m]
\bar{y}	: Dimensionless normal distance
Be	: Bejan number
Br	: Brinkman number = $Ec \times Pr$
Da	: Darcy Number = K / h^2

Ec	: Eckert number = $u_{av}^2 c_p / \Delta T$ or = $u_{max}^2 c_p / \Delta T$
Ha	: Hartman number = $Bh\sqrt{\sigma/\mu}$
Pe	: Peclet number = $Re \times Pr$
Pr	: Prandtl number = $\mu c_p / k$
Re	: Reynolds number = $\rho h^2 g / (\mu u_{av})$ or = $\rho h^2 g / (\mu u_{max})$
α	: Thermal diffusivity [m^2 / s]
θ	: Inclination angle of channel [degree]
μ	: Dynamic viscosity [$Pa \cdot s$]
ρ	: Density of the fluid [kg / m^3]
σ	: Electric conductivity [$(\Omega m)^{-1}$]
$\tau_{i,j}$: Stress tensor
Φ_{vis}	: Viscous dissipation term
Ω	: Dimensionless temperature difference = $\Delta T / T_0$

EFFECT OF POROUS MEDIUM AND MAGNETIC FIELD ON ENTROPY GENERATION OF AN INCOMPRESSIBLE FLOW IN AN INCLINED CHANNEL

SUMMARY

In this thesis, entropy generation due to a gravity-driven, laminar, viscous incompressible fluid flow including viscous dissipation effects through an inclined channel in the presence of a uniform porous-medium and magnetic field is investigated. Fully developed flow field is solved analytically for a Newtonian fluid. Temperature field is numerically obtained by using Finite Difference Method (FDM) and the correctness of the method compared with other sources where applicable. The boundary conditions are considered at both walls to be both constant temperature and constant flux. For the solutions of governing equations certain values for some parameters such as Brinkman number (Br), Darcy number (Da) and Hartmann number (Ha) are assigned and these equation's behaviour under the change of the parameters is also investigated. Entropy generation number (N_s) and Bejan Number (Be) are derived, and plotted using dimensionless velocity and temperature profiles and its change under of the Peclet number (Pe), Group parameter ($Br\Omega^{-1}$), Darcy number and Hartmann number is studied. The effect of heat generation caused by viscous dissipation on the temperature field as well as on the entropy generation is included in the analysis and the results are graphically presented with physical interpretations. In previous similar studies the entropy generation due to viscous dissipation is omitted in inclined channel filled porous medium, whereas this study, as the first time, extends the related literature by considering and interpreting this effect.

EĞİK KANALDA SIKIŞTIRILAMAZ AKIŞTA GÖZENEKLİ ORTAM VE MANYETİK ALAN ŞARTLARININ ENTROPİ ÜRETİMİNE ETKİSİ

ÖZET

Bu çalışmada kütleçekimi tarafından sürülen, laminar, viskoz, sıkıştırılamaz, viskoz yayılma etkileri de gözönüne alınarak tekdüze gözenekli eğimli bir kanalda manyetik etkilerin de varolduğu durumda entropi üretimi incelendi. Newtonien akışkan için tam gelişmiş akış kabulü altındaki bünye denklemleri analitik olarak çözüldü. Sıcaklık alanı Sonlu Farklar Metodu kullanılarak sayısal olarak elde edildi ve doğruluğu uygun yerlerde değişik numerik sonuçlar ile kıyaslandı. Sınır koşulları her durum için iki tane olmak üzere sabit sıcaklık ve sabit ısı akısı olarak alınarak çözüldü. Bünye denklemlerinin çözümü için çeşitli Brinkman sayısı (Br), Darcy sayısı (Da), Hartmann sayısı (Ha) atandı ve denklemlerin bu parametrelerin değişimi sonucundaki davranışı da incelendi. Entropy üretimi sayısı (N_s) ve Bejan sayısı (Be) türetildi ve boyutsuz hız ve sıcaklık profilleri kullanılarak Peclet sayısı (Pe), Brinkman grup parametresi ($Br\Omega^{-1}$), Darcy sayısı ve Hartmann sayısı altındaki değişimleri incelendi. Viskoz yayılma etkisi hem sıcaklık alanı hem de entropi oluşumu denklemlerinde hesaba katıldı ve sonuçlar grafikler ve fiziksel yorumlar ile birlikte sunuldu. Daha önceki benzer gözenekli ortamın mevcut olduğu eğik kanal çalışmalarında viskoz yayılmanın sıcaklık alanı üzerindeki etkisi ihmal edilmiştir; burada ise ilk kez mevzu bahis etkiler göz önüne alınarak literatüre katkıda bulunulmuştur.

1. INTRODUCTION

Natural convection in porous media has a continuously expanding volume of study due to the day by day improvements of thermal engineering applications in industrial life. This breath taking industrialization brings shortages in energy sources and waste of energy. Therefore last three decades emerged on increased awareness that the world energy resources are limited which has caused the political environment almost in all countries to re-examine their energy policies. And the governments working on it have felt to take drastic measures in eliminating waste. It has also started interest in scientific community both to take a closer look at the energy conversion devices and to develop new techniques and analysis methods to better utilize the existing limited resources. Therefore all the energy producing, converting and consuming systems must be re-examined carefully and all possible available-work destruction mechanisms removed. In the theoretical side this can only be done by utilizing Second Law of Thermodynamics, which is related to entropy generation.

Efficiency calculation of heat transfer systems has been very much restricted to the First Law of Thermodynamics. However, calculations using the Second Law of Thermodynamics, which is related to entropy generation and efficiency calculation, are more reliable than first law-based calculations. As entropy generation takes place, the quality of energy decreases. In almost all thermal systems, second law-based efficiency can be defined in terms of the ratio of actual thermal efficiency to reversible thermal efficiency under same conditions. Therefore, the Second Law of Thermodynamics can be applied to investigate the irreversibility in terms of the entropy generation. The determination of entropy generation is also important to enhance the system performance because the entropy generation is the measure of the destruction of the available work of the system [1]. The entropy generation method as a measure of system performance was first introduced by Bejan in 1980 [2], since then many studies have been published on the Second Law of Thermodynamics, entropy generation and the irreversibility of basic arrangements. One of such essential basic arrangement is the channel type geometry flow. For

horizontal channel case, geometry related boundary and symmetry conditions result in having, in most cases, an exact analytical solution. And inclined channel type flow field equations also, though little more difficult than horizontal channel, has some exact solutions. These types of flow fields find wide application in engineering, particularly in heating and cooling areas. In regarding of irreversibility and entropy generation mechanisms, in the inclined type geometries the following studies can be found in open literature, as a short review, as follows; Saouli and Aiboud-Saouli [3] investigated heat transfer of a laminar falling liquid film along an inclined heated plate for a Newtonian fluid via Second Law analysis. They considered the upper surface of the liquid film free and the lower wall fixed with constant heat flux. In another study, Makinde et al. examined the application of Second Law of Thermodynamics to laminar flow of an incompressible viscous fluid through an inclined channel with isothermal walls [4]. In their study, based on some simplifying assumptions and using separation of variables, analytical solutions for the fluid velocity and temperature were constructed.

Makinde investigated heat transfer irreversibility along an inclined plate that is subjected to a prescribed uniform wall temperature [1]. Havzalı et. al. are investigated entropy generation due to the gravity driven laminar viscous incompressible fluid through an inclined channel and in their study, detailed flow and thermal analysis of the entrance section are also outlined [5].

Flow through porous media takes places and the investigation of this phenomenon plays a significant role in various applications like, grain storage, drying process [6], oil recovery [7], heat exchangers and geothermal energy systems [8]. The recent studies in open literature indicate that many researchers and engineers have started working on convective flow and heat transfer in a fluid superposed porous medium with channel geometry. This type of physical system is encountered in many areas like geophysics and engineering applications. The developments in high speed technology forced the investigation of porous media for decreasing the temperatures of chip environment such as in cooling of electronic systems. Some of the problems occur in these applications involve continuous fluid zone and porous zone. In most of the investigations, the fluid used is Newtonian since this type of fluid is very common in nature and practical applications.

In the last two decades, numerous works have been carried out in order to investigate the effects of flow parameters on different geometries for natural convection in filled porous materials. The following studies are related to the filled porous material medium. Baytas [9] studied the natural convection in an inclined porous cavity. In this work the heat transfer is analyzed by solving the balance equations of mass numerically, momentum and energy by Darcy's law and Boussinesq-incompressible approximation. Mahmud and Fraser presented a non-Darcy model for momentum and energy equations in order to calculate the forced convection in a channel filled with a fluid-saturated porous medium [10]. Makinde and Osalusi investigated the laminar flow through a channel filled with saturated porous media by using the Brinkman model. They obtained the velocity and temperature profiles for large Darcy numbers [11]. Alkam, Al-Nimr and Hamdan studied the forced convection flow inside a channel which has parallel plates and it is filled with two porous layers with the same thickness [12]. Nield and Bejan have performed an extensive work on convection in porous media [13]. Al-Nimr and Haddad have studied the convective flow and heat transfer in vertical channels [14]. Shokouhmand, Jam and Salimpour investigated the effects of various parameters like porous medium thickness and Darcy number on the conduit thermal performance accordingly they found that all these parameters had significant influence on the thermal performance of the channel [15]. Paul and Singh used the Brinkman-extended Darcy model to represent momentum transfer in the porous region [16].

The natural convection in an inclined geometry filled with porous medium has been investigated by many other authors i.e., Vasseur et al. [17], Sen et al. [18], Aydin et al. [19].

Meanwhile a great deal of information is available dealing with the generated entropy due to heat and fluid flow in a porous medium [20, 21, 22, 23, 24, 25]. Hooman and Ejlali reported a numerical study by investigating both the First and the Second Law of Thermodynamics for thermally developing forced convection in a circular tube filled by a saturated porous medium including viscous dissipation effects [24]. The entropy generation in a laminar flow through a channel filled with saturated porous media is also investigated by Makinde and Osalusi [26]. Tasnim et al. gave a detailed analysis of entropy generation and the source of irreversibility in a vertical, porous media with transverse hydromagnetic effect for a mixed convective

flow [27]. The problem of entropy generation in a fluid-saturated porous cavity for laminar magnetohydrodynamic natural convection heat transfer was analyzed by Mahmud and Fraser [28]. In a similar study, Mahmud and Fraser [29] analyzed first and second law aspects of fluid flow and heat transfer inside a vertical porous channel with a transverse magnetic field.

1.1 Purpose Of The Thesis

In the view of the preceding studies it can be easily notice that; the flow, temperature, and entropy generation fields in an inclined channel composed of porous materials subjected to natural convection with constant flux at the walls, additionally including viscous dissipation, have not been all studied in a single work yet. In this study the flow field is modelled for a Newtonian fluid and applying the no slip condition at the walls. Then the governing equations of both flow and temperature field for a gravity-driven laminar viscous, incompressible fluid through an inclined channel are reduced to simple ordinary differential equations. While the flow equation is solved analytically, the temperature field equation is solved by the Finite Difference Method (FDM). Despite of the many studies of flow and temperature fields for various types of inclined-channel problems, as referred before, none of them considered the inclined channel with porous medium and viscous dissipation effect interactions.

Additionally, in this study the evaluation of entropy generation and its characteristics depending on the some flow parameters have been presented in great detail. These parameters are Darcy number (Da), Brinkman number (Br) and Peclet number (Pe).

2. THEORY

2.1 Non-dimensionalizations and Dimensionless Parameters

The non-dimensionalizations used in this work is given as follows:

The non-dimensional axial distance:

$$\bar{x} = \frac{x}{Pe h} \quad (2.1)$$

Where Pe is Peclet number and it is detailed in section 2.1.1.

The non-dimensional normal distance:

$$\bar{y} = \frac{y}{h} \quad (2.2)$$

The non-dimensional velocity:

$$\bar{u} = \frac{u}{u_{\max}} \quad (2.3)$$

Where $u_{\max} = u_{@y=0}$ for clear flow case (see section 2.3.1), or:

$$\bar{u} = \frac{u}{u_{av}} \quad (2.4)$$

Where

$$u_{av} = \frac{1}{h - (-h)} \int_{-h}^h u(y) dy \quad (2.5)$$

for the other cases. The non-dimensional temperature:

$$\bar{T} = \frac{T - T_0}{\Delta T} \quad (2.6)$$

where T_0 is the reference temperature, moreover,

$$\Delta T = T_w - T_0 \quad (2.7)$$

for Dirichlet boundary conditions and

$$\Delta T = \frac{qh}{k} \quad (2.8)$$

for Neumann boundary conditions. Also a dimensionless temperature difference is defined as follows:

$$\Omega = \frac{\Delta T}{T_0} \quad (2.9)$$

2.1.1 Peclet Number

Peclet number is a dimensionless number and is defined as the ratio of advection of heat and conduction of heat [30], namely [1]:

$$Pe = \frac{u_{av} \rho c_p h}{k} \text{ or } = \frac{u_{max} \rho c_p h}{k} \quad (2.10)$$

2.1.2 Brinkman Number

Brinkman number is a dimensionless group parameter and is defined as the heat conduction from a wall to a flowing viscous fluid [31] and it is given as follows [1]:

$$Br = \frac{\mu u_{av}^2}{k \Delta T} \text{ or } = \frac{\mu u_{max}^2}{k \Delta T} \quad (2.11)$$

2.1.3 Darcy Number

Darcy number is a dimensionless parameter used in flows in porous media. It is the ratio of permeability of the porous medium and area in which the flow occurs and it is defined as follows [10]:

$$Da = \frac{K}{h^2} \quad (2.12)$$

2.1.4 Hartmann Number

Hartmann number is related to the ratio of drag forces caused by the magnetic induction of the fluid to the viscous forces of the fluid [32] and it is defined as follows [33]:

$$Ha = Bh\sqrt{\frac{\sigma}{\mu}} \quad (2.13)$$

2.2 Continuity Equation

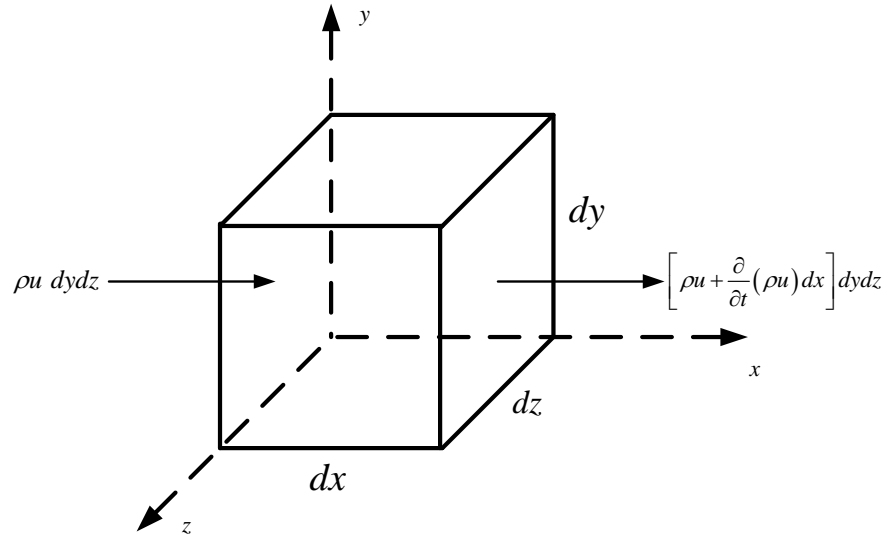


Figure 2.1 : Differential control volume and mass inlet-outlet in x direction

Mass equivalance depending the x ,y and z direciton is tabulated in Table 2.1 below:

Table 2.1: Inlet and outlet of a differential control volume

Inlet	Outlet
x-direction: $\rho u \, dydz$	$\left[\rho u + \frac{\partial}{\partial x}(\rho u) dx \right] dydz$
y- direction: $\rho v \, dxdz$	$\left[\rho v + \frac{\partial}{\partial y}(\rho v) dy \right] dxdz$
z- direction: $\rho w \, dxdy$	$\left[\rho w + \frac{\partial}{\partial z}(\rho w) dz \right] dxdy$

Using the table we can derive the continuity equation for a differential control volume as follows [34]:

$$\frac{\partial \rho}{\partial t} + \frac{\partial}{\partial x}(\rho u) + \frac{\partial}{\partial y}(\rho v) + \frac{\partial}{\partial z}(\rho w) = 0 \text{ and } \vec{\nabla} = \frac{\partial}{\partial x} \hat{i} + \frac{\partial}{\partial y} \hat{j} + \frac{\partial}{\partial z} \hat{k} \quad (2.14)$$

$$\Rightarrow \frac{\partial \rho}{\partial t} + \frac{\partial}{\partial x}(\rho u) + \frac{\partial}{\partial y}(\rho v) + \frac{\partial}{\partial z}(\rho w) \equiv \vec{\nabla} \cdot (\rho \vec{V}) \quad (2.15)$$

Then the equation of continuity becomes as follows:

$$\frac{\partial \rho}{\partial t} + \vec{\nabla} \cdot (\rho \vec{V}) = 0 \quad (2.16)$$

In steady state the equation becomes:

$$\frac{\partial(.)}{\partial t} = 0 \Rightarrow \frac{\partial \rho}{\partial t} = 0 \quad (2.17)$$

Under incompressible assumption the equation is as follows:

$$\vec{\nabla} \cdot \vec{V} = 0 \Rightarrow \frac{\partial u}{\partial x} + \frac{\partial v}{\partial y} + \frac{\partial w}{\partial z} = 0 \quad (2.18)$$

Due to the assumptions of the channel being sufficiently deep in z direction and that there is no transfer between layers, which can be written as:

$$v = w = 0 \quad (2.19)$$

Then the equation of continuity becomes as follows:

$$\frac{\partial u}{\partial x} = 0 \quad (2.20)$$

2.3 Momentum Equation

A general form of the momentum equation is as follows [35]:

$$\rho \vec{g} - \vec{\nabla} p + \vec{\nabla} \cdot \vec{\tau}_{ij} = \rho \frac{d\vec{V}}{dt} \quad (2.21)$$

In other words:

$$\left(\begin{array}{c} \text{gravitation} \\ \text{acting on} \\ \text{unit volume} \end{array} \right) + \left(\begin{array}{c} \text{pressure force} \\ \text{acting on} \\ \text{unit volume} \end{array} \right) + \left(\begin{array}{c} \text{viscous forces} \\ \text{acing on} \\ \text{unit volume} \end{array} \right) = (\text{density} \cdot \text{acceleration})$$

This vectorel equation can be written in a more open form as follows:

x-component

$$\rho g_x - \frac{\partial p}{\partial x} + \frac{\partial \tau_{xx}}{\partial x} + \frac{\partial \tau_{yx}}{\partial y} + \frac{\partial \tau_{zx}}{\partial z} = \rho \left(\frac{\partial u}{\partial t} + u \frac{\partial u}{\partial x} + v \frac{\partial u}{\partial y} + w \frac{\partial u}{\partial z} \right) \quad (2.22)$$

y-component:

$$\rho g_y - \frac{\partial p}{\partial y} + \frac{\partial \tau_{xy}}{\partial x} + \frac{\partial \tau_{yy}}{\partial y} + \frac{\partial \tau_{zy}}{\partial z} = \rho \left(\frac{\partial v}{\partial t} + u \frac{\partial v}{\partial x} + v \frac{\partial v}{\partial y} + w \frac{\partial v}{\partial z} \right) \quad (2.23)$$

z-component:

$$\rho g_z - \frac{\partial p}{\partial z} + \frac{\partial \tau_{xz}}{\partial x} + \frac{\partial \tau_{yz}}{\partial y} + \frac{\partial \tau_{zz}}{\partial z} = \rho \left(\frac{\partial w}{\partial t} + u \frac{\partial w}{\partial x} + v \frac{\partial w}{\partial y} + w \frac{\partial w}{\partial z} \right) \quad (2.24)$$

Due to the fact that we are concerning about Newtonain fluids the following terms will be used for cartesian coordinate system:

$$\tau_{xx} = 2\mu \frac{\partial u}{\partial x} \quad (2.25)$$

$$\tau_{yy} = 2\mu \frac{\partial v}{\partial y} \quad (2.26)$$

$$\tau_{zz} = 2\mu \frac{\partial w}{\partial z} \quad (2.27)$$

$$\tau_{xy} = \tau_{yx} = \mu \left(\frac{\partial u}{\partial y} + \frac{\partial v}{\partial x} \right) \quad (2.28)$$

$$\tau_{xz} = \tau_{zx} = \mu \left(\frac{\partial u}{\partial z} + \frac{\partial w}{\partial x} \right) \quad (2.29)$$

$$\tau_{yz} = \tau_{zy} = \mu \left(\frac{\partial v}{\partial z} + \frac{\partial w}{\partial y} \right) \quad (2.30)$$

In this case conservation of momentum equation for Newtonian fluids is obtained as follows:

x-component:

$$\rho g_x - \frac{\partial p}{\partial x} + \left(\frac{\partial^2 u}{\partial x^2} + \frac{\partial^2 u}{\partial y^2} + \frac{\partial^2 u}{\partial z^2} \right) = \rho \frac{du}{dt} \quad (2.31)$$

y-component:

$$\rho g_y - \frac{\partial p}{\partial y} + \left(\frac{\partial^2 v}{\partial x^2} + \frac{\partial^2 v}{\partial y^2} + \frac{\partial^2 v}{\partial z^2} \right) = \rho \frac{dv}{dt} \quad (2.32)$$

z-component:

$$\rho g_z - \frac{\partial p}{\partial z} + \left(\frac{\partial^2 w}{\partial x^2} + \frac{\partial^2 w}{\partial y^2} + \frac{\partial^2 w}{\partial z^2} \right) = \rho \frac{dw}{dt} \quad (2.33)$$

If we assume the channel sufficiently long, then we can ignore entrance end exit conditions. With the use of the continuity equation (2.20) the x-component of momentum equation, which is

$$\rho g_x - \frac{\partial p}{\partial x} + \mu \left(\frac{\partial^2 u}{\partial x^2} + \frac{\partial^2 u}{\partial y^2} + \frac{\partial^2 u}{\partial z^2} \right) = \rho \left(\frac{\partial u}{\partial t} + u \frac{\partial u}{\partial x} + v \frac{\partial u}{\partial y} + w \frac{\partial u}{\partial z} \right) \quad (2.34)$$

It can be reduced to:

$$\rho g_x - \frac{\partial p}{\partial x} + \mu \left(\frac{\partial^2 u}{\partial y^2} + \frac{\partial^2 u}{\partial z^2} \right) = \rho \left(\frac{\partial u}{\partial t} \right) \quad (2.35)$$

Due to steady state assumption the time derivative vanishes. In this case we get the following:

$$-\frac{\partial p}{\partial x} + \mu \left(\frac{\partial^2 u}{\partial y^2} + \frac{\partial^2 u}{\partial z^2} \right) + \rho g_x = 0 \quad (2.36)$$

With the assumption of one dimensional, fully developed flow, we assume:

$$\frac{\partial^2 u}{\partial y^2} \gg \frac{\partial^2 u}{\partial z^2} \quad (2.37)$$

Which means $u = u(y)$. Therefore we obtain the following:

$$-\frac{\partial p}{\partial x} + \mu \left(\frac{\partial^2 u}{\partial y^2} \right) + \rho g_x = 0 \quad (2.38)$$

In this work, the flow is created by gravitation and there is no pressure gradient otherwise. Then the final form of momentum equation becomes as follows:

$$\mu \left(\frac{\partial^2 u}{\partial y^2} \right) + \rho g \sin \theta = 0 \quad (2.39)$$

This is the form of momentum equation for fully-developed, one dimensional, incompressible, viscous, laminar flow for a Newtonian fluid inside an inclined channel [1].

2.3.1 Clear channel

This is the elementary case of this work. There is neither a porous medium inside the channel nor is there a magnetic field acting on the fluid inside the channel. Again the flow is fully developed and therefore one dimensional. The geometry of this case is given in Fig. 2.2:

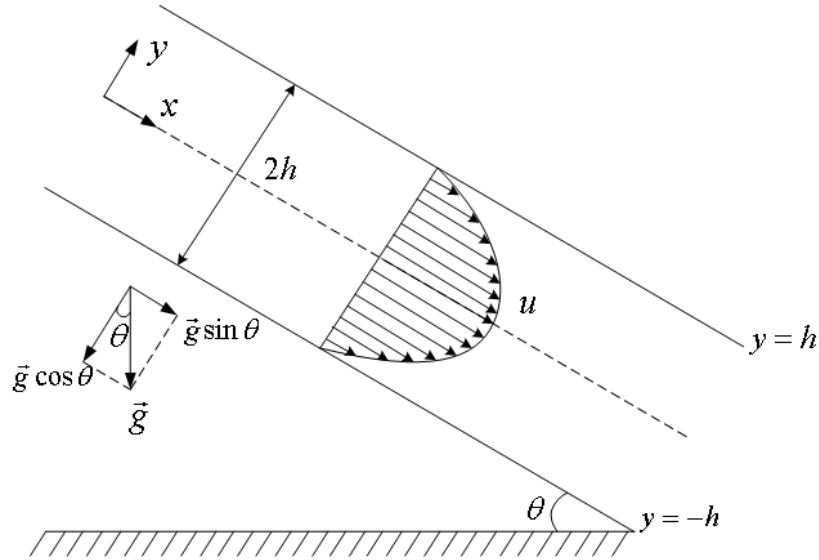


Figure 2.2 : Geometry of clear channel case

The walls are at constant uniform temperature for the Dirichlet problem and there is a uniform constant heat flux at the walls for the Neumann problem.

The boundary conditions for the flow field is given below:

$$u(\pm h) = 0 \quad (2.40)$$

Which is no slip condition at the walls and

$$\left. \frac{du}{dy} \right|_{y=0} = 0 \quad (2.41)$$

Which is symmetry condition at the centre of the channel. Any two of these conditions is necessary and sufficient to solve the differential equation and the solution of (2.39) is obtained as follows:

$$u(y) = \frac{\rho \sin \theta}{2\mu} (h-y)(h+y) \quad (2.42)$$

To obtain a dimensionless form of the equation the non-dimensionalizations given as (2.2) and (2.3) are used together so as to get the dimensionless form of (2.42) as follows:

$$\bar{u}(\bar{y}) = 1 - \bar{y}^2 \quad (2.43)$$

2.3.2 Presence of porous medium

In this case there is an uniform porous medium inside the channel as seen on Fig. 2.3. The third term of the right hand side of (2.44) is related to this phenomenon [26].

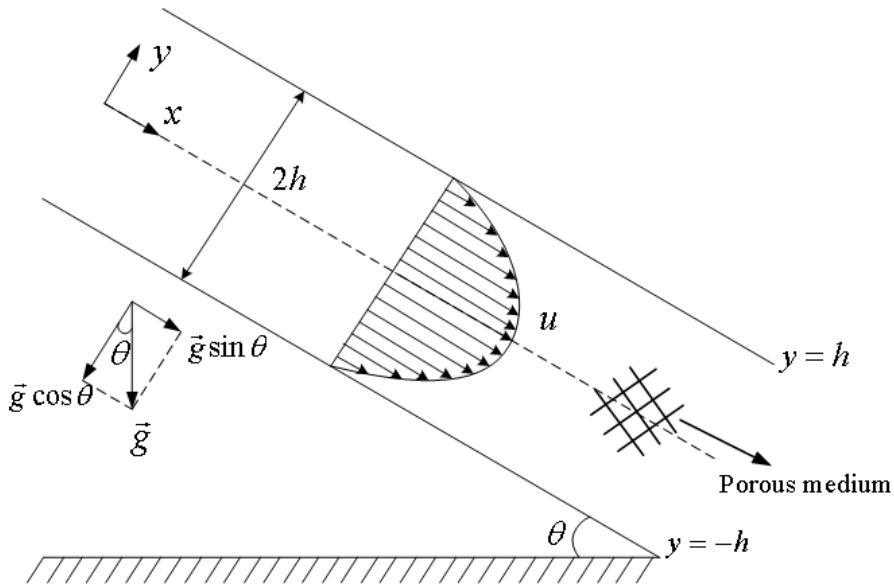


Figure 2.3 : Geometry of the porous case

$$\mu \frac{d^2 u}{dy^2} + \rho g \sin \theta - \frac{\mu}{K} u = 0 \quad (2.44)$$

When equation (2.44) is solved by the boundary conditions given as (2.40) and (2.41) the result is obtained as follows:

$$u(y) = \frac{K \rho \sin \theta}{\mu} \left[1 - \cosh\left(\frac{y}{\sqrt{K}}\right) \operatorname{sech}\left(\frac{h}{\sqrt{K}}\right) \right] \quad (2.45)$$

Which is non-dimensionalized using (2.2), (2.4), (2.5) and (2.12) to result as follows:

$$\frac{u(y)}{u_{av}} = \bar{u}(\bar{y}) = \frac{\cosh\left(\frac{1}{\sqrt{Da}}\right) - \cosh\left(\frac{\bar{y}}{\sqrt{Da}}\right)}{\cosh\left(\frac{1}{\sqrt{Da}}\right) - \sqrt{Da} \sinh\left(\frac{1}{\sqrt{Da}}\right)} \quad (2.46)$$

2.3.3 Presence of magnetic field

In this case there is an uniform magnetic field acting on the fluid inside the channel perpendicular to the channel as seen on Fig. 2.4. The third term of the right hand side of (2.47) is related to this phenomenon [33].

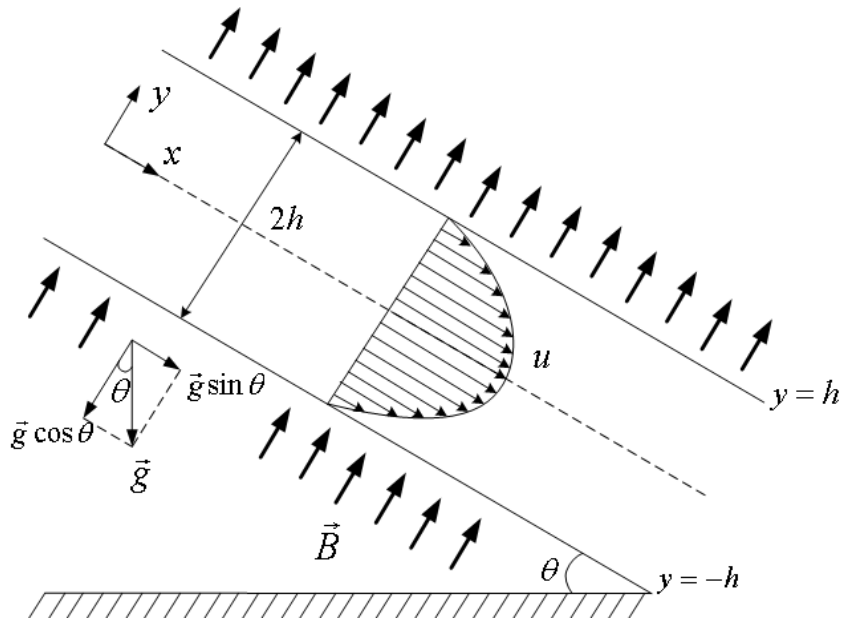


Figure 2.4 : Geometry of the magnetic field case

$$\mu \frac{d^2 u}{dy^2} + \rho g \sin \theta - \sigma B^2 u = 0 \quad (2.47)$$

When equation (2.47) is solved by the boundary conditions given as (2.40) and (2.41) the result is obtained as follows:

$$u(y) = \frac{\rho \sin \theta}{B^2 \sigma} \left[1 - \cosh \left(B \sqrt{\frac{\sigma}{\mu}} y \right) \operatorname{sech} \left(Bh \sqrt{\frac{\sigma}{\mu}} \right) \right] \quad (2.48)$$

Which is non-dimensionalized using, (2.4), (2.5) and (2.13) to result as follows:

$$\frac{u(y)}{u_{av}} = \bar{u}(\bar{y}) = \frac{Ha \left[-1 + \cosh(Ha \bar{y}) \operatorname{sech}(Ha) \right]}{-Ha + \tanh(Ha)} \quad (2.49)$$

2.3.4 Presence of both porous medium and magnetic field

In this case there is both uniform porous medium inside the channel and a uniform magnetic field perpendicular to the channel as seen on Fig 2.5.

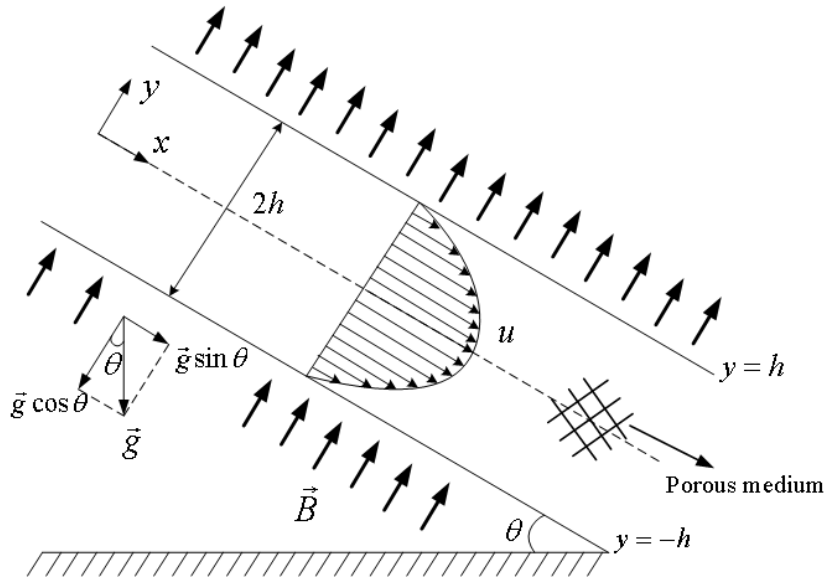


Figure 2.5 : Geometry for both porous and magnetic case

$$\mu \frac{d^2 u}{dy^2} + \rho g \sin \theta - \sigma B^2 u - \frac{\mu}{K} u = 0 \quad (2.50)$$

When equation (2.50) is solved by the boundary conditions given as (2.40) and (2.41) the result is obtained as follows:

$$u(y) = \frac{\rho g \sin \theta}{\frac{\mu}{K} + B^2 \sigma} \left[1 - \cosh \left(y \sqrt{\frac{1}{K} + \frac{B^2 \sigma}{\mu}} \right) \operatorname{sech} \left(h \sqrt{\frac{1}{K} + \frac{B^2 \sigma}{\mu}} \right) \right] \quad (2.51)$$

Which is non-dimensionalized using, (2.4), (2.5), (2.12) and (2.13) and to result as follows:

$$\frac{u(y)}{u_{av}} = \bar{u}(\bar{y}) = \frac{\sqrt{\frac{1}{Da + Ha^2}} \left[1 - \cosh \left(\bar{y} \sqrt{\frac{1}{Da + Ha^2}} \right) \operatorname{sech} \left(\sqrt{\frac{1}{Da + Ha^2}} \right) \right]}{\sqrt{\frac{1}{Da + Ha^2}} - \tanh \left(\sqrt{\frac{1}{Da + Ha^2}} \right)} \quad (2.52)$$

2.4 Energy Equation

A general form of energy equation is given in [37] as follows:

$$\rho c_p \left(\frac{\partial T}{\partial t} + \vec{V} \cdot \nabla T \right) = k \nabla^2 T + \dot{q} \quad (2.53)$$

Where the first term in brackets is called energy storage, the second term in brackets is called enthalpy convection; the first term on the right hand side of the equation is called heat conduction and the second term on the right hand side of the equation is called heat generation. Here, the term in paranthesis can also be written as follows:

$$\frac{DT}{Dt} \equiv \frac{\partial T}{\partial t} + \vec{V} \cdot \nabla T = \frac{\partial T}{\partial t} + u \frac{\partial T}{\partial x} + v \frac{\partial T}{\partial y} + w \frac{\partial T}{\partial z} \quad (2.54)$$

Which is the material derivative. For a steady state, two dimensional flow with no heat generation inside the fluid along with the condition in (2.19) this equation reduces to the following:

$$u \frac{\partial T}{\partial x} = \alpha \frac{\partial^2 T}{\partial y^2} \quad (2.55)$$

Which can be non-dimensionalized by (2.1), (2.2), (2.3), (2.6), (2.7) and (2.10) as follows:

$$\bar{u} \frac{\partial \bar{T}}{\partial \bar{x}} = \frac{\partial^2 \bar{T}}{\partial \bar{y}^2} \quad (2.56)$$

The boundary conditions of the energy equation is given in (2.55) are as seen on (2.57) and (2.58).

For the dirichlet cases, entrance condition:

$$T(0, y) = 0 \quad (2.57)$$

Uniformly distributed temperature on the wall of the inclined channel is as follows:

$$T(x, h) = T(x, -h) = T_w \quad (2.58)$$

which are non-dimensionalized with (2.1), (2.2), (2.10) (2.6) and (2.7) as (2.59) and (2.60).

Entrance condition:

$$\bar{T}(0, \bar{y}) = 0 \quad (2.59)$$

Uniformly distributed temperature on the wall of the inclined channel is as follows:

$$\bar{T}(\bar{x}, 1) = \bar{T}(\bar{x}, -1) = 1 \quad (2.60)$$

As for the Neumann cases, entrance condition:

$$T(0, y) = 0 \quad (2.61)$$

Uniformly distributed flux on the wall to the inclined channel is as follows:

$$-k \frac{\partial T(x, -h)}{\partial y} = -k \frac{\partial T(x, h)}{\partial y} = q \quad (2.62)$$

which are non-dimensionalized with (2.1), (2.2), (2.10) (2.6) and (2.8) as (2.63) and (2.64) below.

Entrance condition:

$$\bar{T}(0, \bar{y}) = 0 \quad (2.63)$$

Uniformly distributed flux on the wall to the inclined channel is as follows:

$$\frac{\partial}{\partial \bar{y}} \bar{T}(\bar{x}, -1) = \frac{\partial}{\partial \bar{y}} \bar{T}(\bar{x}, 1) = -1 \quad (2.64)$$

2.4.1 Clear channel

For a steady state, two dimensional flow with no heat generation inside the fluid for an one dimensional, viscous, incompressible flow with viscous dissipation is given as follows:

$$u \frac{\partial T}{\partial x} = \frac{k}{\rho c_p} \frac{\partial^2 T}{\partial y^2} + \frac{\mu}{\rho c_p} \left(\frac{du}{dy} \right)^2 \quad (2.65)$$

Here the second term of the right hand side of the equation is called the viscous dissipation term [33]. Equation (2.65) can be non-dimensionalized with (2.1), (2.2), (2.3), (2.6), and (2.11) along with (2.7) and (2.8) for Dirichlet and for Neumann case respectively, as follows:

$$\bar{u} \frac{\partial \bar{T}}{\partial \bar{x}} = \frac{\partial^2 \bar{T}}{\partial \bar{y}^2} + Br \left(\frac{\partial \bar{u}}{\partial \bar{y}} \right)^2 \quad (2.66)$$

2.4.2 Presence of porous medium

In this case there is a porous medium inside the channel and the last term of the right hand side of the following equation is related to porosity inside the channel [25].

$$u \frac{\partial T}{\partial x} = \frac{k}{\rho c_p} \frac{\partial^2 T}{\partial y^2} + \frac{\mu}{\rho c_p} \left(\frac{du}{dy} \right)^2 + \frac{\mu}{\rho c_p K} u^2 \quad (2.67)$$

Equation (2.67) can be non-dimensionalized with (2.1), (2.2), (2.3), (2.6), (2.11) and (2.12) along with (2.7) and (2.8) for Dirichlet and for Neumann case respectively, as follows:

$$\bar{u} \frac{\partial \bar{T}}{\partial \bar{x}} = \frac{\partial^2 \bar{T}}{\partial \bar{y}^2} + Br \left(\frac{\partial \bar{u}}{\partial \bar{y}} \right)^2 + \frac{Br}{Da} \bar{u}^2 \quad (2.68)$$

2.4.3 Presence of magnetic field

In this case there is a magnetic field perpendicular to the channel and the last term of the right hand side of the following equation is related to porosity inside the channel [33].

$$u \frac{\partial T}{\partial x} = \frac{k}{\rho c_p} \frac{\partial^2 T}{\partial y^2} + \frac{\mu}{\rho c_p} \left(\frac{du}{dy} \right)^2 + \frac{\sigma B^2}{\rho c_p} u^2 \quad (2.69)$$

Equation (2.69) can be non-dimensionalized with (2.1), (2.2), (2.3), (2.6), (2.11) and (2.13) along with (2.7) and (2.8) for Dirichlet and for Neumann case respectively, as follows:

$$\bar{u} \frac{\partial \bar{T}}{\partial \bar{x}} = \frac{\partial^2 \bar{T}}{\partial \bar{y}^2} + Br \left(\frac{\partial \bar{u}}{\partial \bar{y}} \right)^2 + Ha^2 Br \bar{u}^2 \quad (2.70)$$

2.4.4 Presence of both porous medium and magnetic field

In this case there is both a uniform porous medium and a magnetic field perpendicular to the channel and the last term of the right hand side of the following equation is related to porosity inside the channel.

$$u \frac{\partial T}{\partial x} = \frac{k}{\rho c_p} \frac{\partial^2 T}{\partial y^2} + \frac{\mu}{\rho c_p} \left(\frac{du}{dy} \right)^2 + \frac{\mu}{\rho c_p K} u^2 + \frac{\sigma B^2}{\rho c_p} u^2 \quad (2.71)$$

Equation (2.67) can be non-dimensionalized with (2.1), (2.2), (2.3), (2.6), (2.11), (2.12) and (2.13) along with (2.7) and (2.8) for Dirichlet and for Neumann case respectively, as follows:

$$\bar{u} \frac{\partial \bar{T}}{\partial \bar{x}} = \frac{\partial^2 \bar{T}}{\partial \bar{y}^2} + Br \left(\frac{\partial \bar{u}}{\partial \bar{y}} \right)^2 + \frac{Br}{Da} \bar{u}^2 + Ha^2 Br \bar{u}^2 \quad (2.72)$$

2.5 Entropy Generation

In Fig. 2.6 there is an open thermodynamic system which is not closed to the effects of mass flux, energy transfer and entropy transfer with an area of $dx \, dy$.

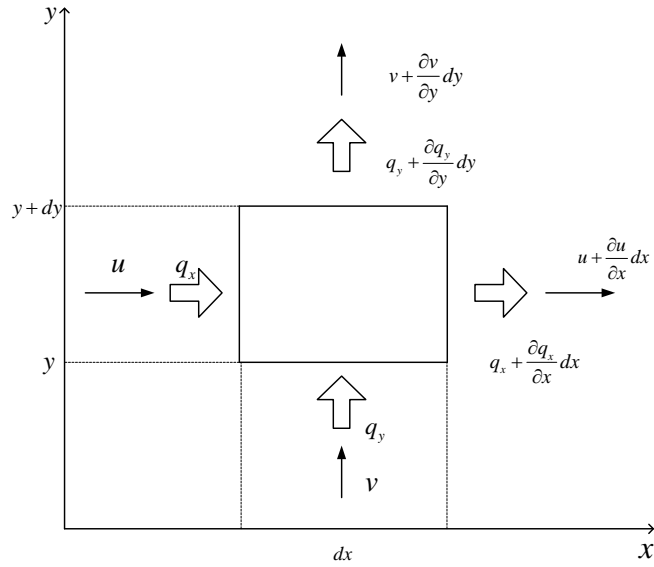


Figure 2.6 : Local entropy generation by convection heat transfer

Since the area is small the mass distribution inside it can be assumed uniform, therefore unit entropy generation for unit volume is as follows:

$$\begin{aligned}
 S_G dx dy = & \left[\frac{q_x + \frac{\partial q_x}{\partial x} dx}{T + \frac{\partial T}{\partial x} dx} + \frac{q_y + \frac{\partial q_y}{\partial y} dy}{T + \frac{\partial T}{\partial y} dy} - \frac{q_x}{T} dy - \frac{q_y}{T} dx \right] \\
 & + \left[\left(s + \frac{\partial s}{\partial x} dx \right) \left(u + \frac{\partial u}{\partial x} dx \right) \left(\rho + \frac{\partial \rho}{\partial x} dx \right) dy \right. \\
 & + \left. \left(s + \frac{\partial s}{\partial y} dy \right) \left(u + \frac{\partial v}{\partial y} dy \right) \left(\rho + \frac{\partial \rho}{\partial y} dy \right) dx - su \rho dy - sv \rho dx \right] \\
 & + \left[\frac{\partial(\rho s)}{\partial t} dx dy \right]
 \end{aligned} \tag{2.73}$$

Here the first four terms in the brackets are entropy transfer related to heat transfer, second four terms in the second bracket are related to the entropy transferred inside and outside of the system and the last term is the time dependent entropy generation inside the control volume. If the relation is divided by $dx dy$ we get the following relation [38]:

$$S_G = \frac{1}{T} \left(\frac{\partial q_x}{\partial x} + \frac{\partial q_y}{\partial y} \right) - \frac{1}{T^2} \left(q_x \frac{\partial T}{\partial x} + q_y \frac{\partial T}{\partial y} \right) + \rho \left(\frac{\partial s}{\partial t} + u \frac{\partial s}{\partial x} + v \frac{\partial s}{\partial y} \right) + s \left[\frac{\partial \rho}{\partial t} + u \frac{\partial \rho}{\partial x} + v \frac{\partial \rho}{\partial y} + \rho \left(\frac{\partial u}{\partial x} + \frac{\partial v}{\partial y} \right) \right] \quad (2.74)$$

Here the fourth term on the right hand side of the equation is the open form of

$$\frac{D\rho}{Dt} + \rho \nabla \cdot \vec{V} = 0 \quad (2.75)$$

and it is equal to zero. Volumetric entropy generation can be written in vector form as follows:

$$S_G = \frac{1}{T} \nabla \cdot \vec{q} - \frac{1}{T^2} \vec{q} \cdot \nabla T + \rho \frac{Ds}{Dt} \quad (2.76)$$

Using the first law of thermodynamics for any point in a convective medium the following can be written:

$$\rho \frac{De}{Dt} = -\nabla \cdot \vec{q} - P(\nabla \cdot \vec{V}) + \mu \Phi_{vis} \quad (2.77)$$

Here the internal energy for unit volume is equal to the sum of heat transfer due to conduction, work transfer due to compression and work transfer due to viscous dissipation for unit volume. Using the following relation:

$$de = Tds - Pd(1/\rho) \quad (2.78)$$

we can write the following relation:

$$\rho \frac{Ds}{Dt} = \frac{\rho}{T} \frac{De}{Dt} - \frac{P}{\rho T} \frac{D\rho}{Dt} \quad (2.79)$$

Using (2.79) along with (2.74) we can write the following:

$$S_G = -\frac{1}{T^2} \vec{q} \cdot \nabla T + \frac{\mu}{T} \Phi_{vis} \quad (2.80)$$

If Fourier's law of heat conduction ($\vec{q} = -k\nabla T$) is used for an isotropic medium the volumetric entropy generation becomes as follows:

$$S_G = \frac{k}{T^2} (\nabla T)^2 + \frac{\mu}{T} \Phi_{vis} \quad (2.81)$$

Here Φ_{vis} is as follows [39]:

$$\Phi_{vis} = 2 \left[\left(\frac{\partial u}{\partial x} \right)^2 + \left(\frac{\partial v}{\partial y} \right)^2 + \left(\frac{\partial w}{\partial z} \right)^2 \right] + \left[\left(\frac{\partial u}{\partial y} + \frac{\partial v}{\partial x} \right)^2 + \left(\frac{\partial u}{\partial z} + \frac{\partial w}{\partial y} \right)^2 + \left(\frac{\partial w}{\partial x} + \frac{\partial u}{\partial z} \right)^2 \right] - \frac{2}{3} \left(\frac{\partial u}{\partial x} + \frac{\partial v}{\partial y} + \frac{\partial w}{\partial z} \right)^2 \quad (2.82)$$

In this case (2.81) for a two dimensional cartesian coordinate becomes as follows:

$$S_G = \frac{k}{T^2} \left[\left(\frac{\partial T}{\partial x} \right)^2 + \left(\frac{\partial T}{\partial y} \right)^2 \right] + \frac{\mu}{T} \left\{ 2 \left[\left(\frac{\partial u}{\partial x} \right)^2 + \left(\frac{\partial v}{\partial y} \right)^2 \right] + \left(\frac{\partial u}{\partial x} + \frac{\partial v}{\partial y} \right)^2 \right\} \quad (2.83)$$

For our one dimensional problem, (2.83) reduces to the following relation [41]:

$$S_G = \frac{k}{T_0^2} \left[\left(\frac{\partial T}{\partial x} \right)^2 + \left(\frac{\partial T}{\partial y} \right)^2 \right] + \frac{\mu}{T_0} \left(\frac{\partial u}{\partial y} \right)^2 \quad (2.84)$$

2.5.1 Entropy generation number

Dimensionless entropy generation number is defined as follows [1]:

$$N_s = \frac{h^2 T_0^2 S_G}{k \Delta T^2} \quad (2.85)$$

2.5.2 Bejan number

Bejan number is defined as follows [40]:

$$Be = \frac{N_x + N_y}{N_f + (N_p + N_m)} = \frac{N_h}{N_f + (N_p + N_m)} \quad (2.86)$$

Bejan number is the ratio between heat transfer irreversibility to the total irreversibility occurred within the system. While $Be=1$ the heat transfer irreversibility is dominant. On the other hand if $Be=0$ irreversibility due to fluid friction dominates. If $Be=1/2$ the heat transfer irreversibility and fluid friction irreversibility contributes to the system equally. The terms in the paranthesis is applied where relevant i.e. there is a porous medium and/or magnetic field.

2.5.3 Clear channel

Entropy generation number for clear channel is given as follows [1]:

$$S_G = \frac{k}{T_0^2} \left[\left(\frac{\partial T}{\partial x} \right)^2 + \left(\frac{\partial T}{\partial y} \right)^2 \right] + \frac{\mu}{T_0} \left(\frac{\partial u}{\partial y} \right)^2 \quad (2.87)$$

Equation (2.87) can be non-dimensionalized with (2.85) as follows:

$$N_s = \frac{1}{Pe^2} \left(\frac{\partial \bar{T}}{\partial \bar{x}} \right)^2 + \left(\frac{\partial \bar{T}}{\partial \bar{y}} \right)^2 + \frac{Br}{\Omega} \left(\frac{\partial \bar{u}}{\partial \bar{y}} \right)^2 = N_h + N_f \quad (2.88)$$

Here the third term of the right hand side of the equation comes from viscous dissipation term denoted in (2.82) and simplified in (2.84). The Bejan number for this case is as follows:

$$Be = \frac{N_h}{N_f} \quad (2.89)$$

2.5.4 Presence of porous medium

The entropy generation of the porous case is given as follows [27]:

$$S_G = \frac{k}{T_0^2} \left[\left(\frac{\partial T}{\partial x} \right)^2 + \left(\frac{\partial T}{\partial y} \right)^2 \right] + \frac{\mu}{T_0} \left(\frac{\partial u}{\partial y} \right)^2 + \frac{\mu}{T_0 K} u^2 \quad (2.90)$$

Equation (2.90) can be non-dimensionalized with (2.85) as follows:

$$N_s = \frac{1}{Pe^2} \left(\frac{\partial \bar{T}}{\partial \bar{x}} \right)^2 + \left(\frac{\partial \bar{T}}{\partial \bar{y}} \right)^2 + \frac{Br}{\Omega} \left(\frac{\partial \bar{u}}{\partial \bar{y}} \right)^2 + \frac{Br}{\Omega} \frac{1}{Da} \bar{u}^2 = N_h + N_f + N_p \quad (2.91)$$

Here the fourth term of the right hand side of the equation is entropy generation due to porosity and will be denoted as N_p . The Bejan number for this case is as follows:

$$Be = \frac{N_h}{N_f + N_p} \quad (2.92)$$

2.5.5 Presence of magnetic field

The entropy generation of the porous case is given as follows [27]:

$$S_G = \frac{k}{T_0^2} \left[\left(\frac{\partial T}{\partial x} \right)^2 + \left(\frac{\partial T}{\partial y} \right)^2 \right] + \frac{\mu}{T_0} \left(\frac{\partial u}{\partial y} \right)^2 + \frac{\sigma B^2}{T_0} u^2 \quad (2.93)$$

Equation (2.93) can be non-dimensionalized with (2.85) as follows:

$$N_s = \frac{1}{Pe^2} \left(\frac{\partial \bar{T}}{\partial \bar{x}} \right)^2 + \left(\frac{\partial \bar{T}}{\partial \bar{y}} \right)^2 + \frac{Br}{\Omega} \left(\frac{\partial \bar{u}}{\partial \bar{y}} \right)^2 + \frac{Br}{\Omega} Ha^2 \bar{u}^2 = N_h + N_f + N_m \quad (2.94)$$

Here the fourth term of the right hand side of the equation is entropy generation due to magnetic field and will be denoted as N_m . The Bejan number for this case is as follows:

$$Be = \frac{N_h}{N_f + N_m} \quad (2.95)$$

2.5.6 Presence of both porous medium and magnetic field

The entropy generation of both porous and magnetic field case is given as follows:

$$S_G = \frac{k}{T_0^2} \left[\left(\frac{\partial T}{\partial x} \right)^2 + \left(\frac{\partial T}{\partial y} \right)^2 \right] + \frac{\mu}{T_0} \left(\frac{\partial u}{\partial y} \right)^2 + \frac{\mu}{T_0 K} u^2 + \frac{\sigma B^2}{T_0} u^2 \quad (2.96)$$

Equation (2.96) can be non-dimensionalized with (2.85) as follows:

$$\begin{aligned} N_s &= \frac{1}{Pe^2} \left(\frac{\partial \bar{T}}{\partial \bar{x}} \right)^2 + \left(\frac{\partial \bar{T}}{\partial \bar{y}} \right)^2 + \frac{Br}{\Omega} \left(\frac{\partial \bar{u}}{\partial \bar{y}} \right)^2 + \frac{Br}{\Omega} \frac{1}{Da} \bar{u}^2 + \frac{Br}{\Omega} Ha^2 \bar{u}^2 \\ &= N_h + N_f + N_p + N_m \end{aligned} \quad (2.97)$$

The Bejan number for this case is as follows:

$$Be = \frac{N_h}{N_f + (N_p + N_m)} \quad (2.98)$$

2.6 Solution Methods

2.6.1 Some analytic solutions

The solution to (2.55) which is when considered with velocity profile of the clear case, (2.43) is same type equation as follows [42]:

$$(1-y^2)\frac{\partial\omega}{\partial x} = a\frac{\partial^2\omega}{\partial y^2} \quad (2.99)$$

And solution of this equation for the boundary conditions given in (2.59) and (2.60) is given to (2.99) as follows:

$$\omega(x, y) = 1 - \sum_{m=0}^{\infty} A_m \exp(-a\lambda_m^2 x) G_m(y) \quad (2.100)$$

Where:

$$G_m(y) = \exp\left(-\frac{1}{2}\lambda_m y^2\right) \phi\left(\frac{1}{4} - \frac{1}{4}\lambda_m, \frac{1}{2}; \lambda_m y^2\right);$$

$$\phi(\alpha, \beta; z) = 1 + \sum_{m=1}^{\infty} \frac{\alpha(\alpha+1)\dots(\alpha+m-1)}{\beta(\beta+1)\dots(\beta+m-1)} \frac{z^m}{m!};$$

$$\lambda_m = 4m + 1.68 \quad (m = 0, 1, 2, \dots);$$

$$A_0 = 1.2, A_m = (-1)^m 2.27\lambda_m^{-7/6} \quad (m=1, 2, 3, \dots)$$

Here $\lambda_{m,\text{error}} < 0.2\%$ and $A_{m,\text{error}} < 0.1\%$ has the respective percentage errors.

Another comparison chance rises for magnetic Neumann case. A similar problem analytically solved by Aiboud-Saouli et. al. [43]. The solution for (2.70) is given as follows:

$$\begin{aligned} \Theta(X, Y) = & \alpha X + \frac{\alpha}{(\cosh(Ha) - 1)} \left[\frac{Y^2}{2} \cosh(Ha) - \frac{\cosh(Ha(1-Y))}{Ha^2} \right] \\ & - \frac{BrHa^2}{(\cosh(Ha) - 1)^2} \left[\frac{Y^2}{2} \cosh^2(Ha) - \frac{2}{Ha^2} \cosh(Ha) \right. \\ & \left. \cdot \cosh(Ha(1-Y)) + \frac{1}{4Ha^2} \cosh(2Ha(1-Y)) \right] + C_1 Y + C \end{aligned} \quad (2.101)$$

where α , C_1 and C are constants of integration and are given as follows:

$$\begin{aligned}\alpha &= \frac{A_3 - A_4}{A_1 - A_2}, C_1 = \frac{A_1 A_4 - A_2 A_3}{A_1 - A_2}, \\ A_1 &= \frac{\sinh(Ha)}{Ha(\cosh(Ha) - 1)}, A_2 = \frac{\cosh(Ha)}{\cosh(Ha) - 1} \\ A_3 &= \frac{BrHa^2}{(\cosh(Ha) - 1)^2} \left(\frac{2}{Ha} \cosh(Ha) \sinh(Ha) - \frac{1}{2Ha} \sinh(2Ha) \right) - 1 \\ A_4 &= \frac{BrHa^2 \cosh^2(Ha)}{(\cosh(Ha) - 1)^2}, \\ C &= \frac{\alpha}{(\cosh(Ha) - 1)} \left[\frac{\sinh(Ha)}{Ha^3} \right] - \frac{BrHa^2}{(\cosh(Ha) - 1)^2} \left[\frac{2}{Ha^3} \cosh(Ha) \sinh(Ha) \right. \\ &\quad \left. - \frac{2}{16Ha^3} \sinh(2Ha) \right] - \frac{\alpha}{6(\cosh(Ha) - 1)} + \frac{BrHa^2 \cosh^2(Ha)}{6(\cosh(Ha) - 1)^2} - \frac{C_1}{2}\end{aligned}$$

2.6.2 The core numerical scheme

The core implicit method used in this work is presented as follows:

$$u_i \frac{\bar{T}_{i,j} - \bar{T}_{i-1,j}}{\Delta x} = \frac{\bar{T}_{i,j-1} - 2\bar{T}_{i,j} + \bar{T}_{i,j+1}}{\Delta y^2} + O(\Delta x) + O(\Delta y^2) \quad (2.102)$$

As it can be seen it is backward in x direction and central in y direction. It has a first order truncation error in x direction and second order in y direction. LU decomposition is used for the solution of the set of the equations we obtained using this method. This is the energy equation for clear flow case without viscous dissipation, namely (2.55).

This scheme, the core scheme as it is called in this work, is used for comparative purposes in terms of approximate error for the cases studied. It is compared both with analytical solution given in (2.100) and numerical differential equation solver NDSolve integrated within Wolfram Mathematica due to the fact that most of the work here is new and there is nothing to compare with in terms of percentage error. The schemes used in the calculation of the cases is given below.

Scheme for the clear case is as follows:

$$u_i \frac{\bar{T}_{i,j} - \bar{T}_{i-1,j}}{\Delta x} = \frac{\bar{T}_{i,j-1} - 2\bar{T}_{i,j} + \bar{T}_{i,j+1}}{\Delta y^2} + Br \left(\frac{\partial \bar{u}}{\partial y} \right)_i^2 + O(\Delta x) + O(\Delta y^2) \quad (2.103)$$

Scheme for the porous case is as follows:

$$u_i \frac{\bar{T}_{i,j} - \bar{T}_{i-1,j}}{\Delta x} = \frac{\bar{T}_{i,j-1} - 2\bar{T}_{i,j} + \bar{T}_{i,j+1}}{\Delta y^2} + Br \left(\frac{\partial \bar{u}}{\partial y} \right)_i^2 + \frac{Br}{Da} \bar{u}_i^2 + O(\Delta x) + O(\Delta y^2) \quad (2.104)$$

Scheme for the magnetic case is as follows:

$$u_i \frac{\bar{T}_{i,j} - \bar{T}_{i-1,j}}{\Delta x} = \frac{\bar{T}_{i,j-1} - 2\bar{T}_{i,j} + \bar{T}_{i,j+1}}{\Delta y^2} + Br \left(\frac{\partial \bar{u}}{\partial y} \right)_i^2 + Ha^2 Br \bar{u}_i^2 + O(\Delta x) + O(\Delta y^2) \quad (2.105)$$

Scheme for the both porous and magnetic case is as follows:

$$u_i \frac{\bar{T}_{i,j} - \bar{T}_{i-1,j}}{\Delta x} = \frac{\bar{T}_{i,j-1} - 2\bar{T}_{i,j} + \bar{T}_{i,j+1}}{\Delta y^2} + Br \left(\frac{\partial \bar{u}}{\partial y} \right)_i^2 + \frac{Br}{Da} \bar{u}_i^2 + Ha^2 Br \bar{u}_i^2 + O(\Delta x) + O(\Delta y^2) \quad (2.106)$$

2.6.2.1 Stability of the core scheme

Let us apply the Von Neumann stability analysis to the core scheme. If we rearrange the FDE we get the following:

$$\bar{T}_{i-1,j} = \bar{T}_{i,j} - \xi (\bar{T}_{i,j-1} - 2\bar{T}_{i,j} + \bar{T}_{i,j+1}) \quad (2.107)$$

Where:

$$\xi = \frac{\Delta x}{u \Delta y^2} \quad (2.108)$$

Let us take the Fourier transform of the FDE:

$$\begin{aligned}
\bar{T}_{i-1,j} &= \bar{T}_{i,j} - \xi (\bar{T}_{i,j-1} - 2\bar{T}_{i,j} + \bar{T}_{i,j+1}) \\
U^{i-1} e^{I\theta j} &= U^i e^{I\theta j} - \xi (U^i e^{I\theta j} e^{-I\theta} - 2U^i e^{I\theta j} + U^i e^{I\theta j} e^{I\theta}) \\
\Rightarrow U^{i-1} &= U^i [1 - \xi (e^{-I\theta} + e^{I\theta} - 2)] \\
\Rightarrow U^{i-1} &= U^i [1 - 2\xi (\cos \theta - 1)] \\
\frac{U^i}{U^{i-1}} &= G = \frac{1}{1 + 2\xi (1 - \cos \theta)} \tag{2.109}
\end{aligned}$$

Where G is the amplification factor. The stability condition is as follows:

$$|G| \leq 1 \tag{2.110}$$

Therefore the scheme is unconditionally stable for $|G|$ will always be smaller than 1.

2.6.2.2 Consistency of the core scheme

For the consistency analysis let us expand each term to Taylor series in our FDE:

$$\begin{aligned}
\bar{T}_{i-1,j} &= \bar{T}_{i,j} - \Delta x \left(\frac{\partial \bar{T}_j}{\partial x} \right)_i + \frac{\Delta x^2}{2} \left(\frac{\partial^2 \bar{T}_j}{\partial x^2} \right)_i - \frac{\Delta x^3}{6} \left(\frac{\partial^3 \bar{T}_j}{\partial x^3} \right)_i + \frac{\Delta x^4}{24} \left(\frac{\partial^4 \bar{T}_j}{\partial x^4} \right)_i \\
\bar{T}_{i,j+1} &= \bar{T}_{i,j} + \Delta y \left(\frac{\partial \bar{T}_j}{\partial y} \right)_i + \frac{\Delta y^2}{2} \left(\frac{\partial^2 \bar{T}_j}{\partial y^2} \right)_i + \frac{\Delta y^3}{6} \left(\frac{\partial^3 \bar{T}_j}{\partial y^3} \right)_i + \frac{\Delta y^4}{24} \left(\frac{\partial^4 \bar{T}_j}{\partial y^4} \right)_i \\
\bar{T}_{i,j-1} &= \bar{T}_{i,j} - \Delta y \left(\frac{\partial \bar{T}_j}{\partial y} \right)_i + \frac{\Delta y^2}{2} \left(\frac{\partial^2 \bar{T}_j}{\partial y^2} \right)_i - \frac{\Delta y^3}{6} \left(\frac{\partial^3 \bar{T}_j}{\partial y^3} \right)_i + \frac{\Delta y^4}{24} \left(\frac{\partial^4 \bar{T}_j}{\partial y^4} \right)_i
\end{aligned}$$

Then the FDE becomes:

$$\begin{aligned}
&\bar{T}_{i,j} - \Delta x \left(\frac{\partial \bar{T}_j}{\partial x} \right)_i + \frac{\Delta x^2}{2} \left(\frac{\partial^2 \bar{T}_j}{\partial x^2} \right)_i - \frac{\Delta x^3}{6} \left(\frac{\partial^3 \bar{T}_j}{\partial x^3} \right)_i + \frac{\Delta x^4}{24} \left(\frac{\partial^4 \bar{T}_j}{\partial x^4} \right)_i \\
&= \bar{T}_{i,j} - \xi \left[\bar{T}_{i,j} - \Delta y \left(\frac{\partial \bar{T}_j}{\partial y} \right)_i + \frac{\Delta y^2}{2} \left(\frac{\partial^2 \bar{T}_j}{\partial y^2} \right)_i - \frac{\Delta y^3}{6} \left(\frac{\partial^3 \bar{T}_j}{\partial y^3} \right)_i + \frac{\Delta y^4}{24} \left(\frac{\partial^4 \bar{T}_j}{\partial y^4} \right)_i \right. \\
&\quad \left. - 2\bar{T}_{i,j} + \bar{T}_{i,j} + \Delta y \left(\frac{\partial \bar{T}_j}{\partial y} \right)_i + \frac{\Delta y^2}{2} \left(\frac{\partial^2 \bar{T}_j}{\partial y^2} \right)_i + \frac{\Delta y^3}{6} \left(\frac{\partial^3 \bar{T}_j}{\partial y^3} \right)_i + \frac{\Delta y^4}{24} \left(\frac{\partial^4 \bar{T}_j}{\partial y^4} \right)_i \right]
\end{aligned}$$

Let us simplify and replace ξ to this expression:

$$\left(\frac{\partial \bar{T}_j}{\partial x} \right)_i + \frac{\Delta x}{2} \left(\frac{\partial^2 \bar{T}_j}{\partial x^2} \right)_i - \frac{\Delta x^2}{6} \left(\frac{\partial^3 \bar{T}_j}{\partial x^3} \right)_i + \frac{\Delta x^3}{24} \left(\frac{\partial^4 \bar{T}_j}{\partial x^4} \right)_i = \frac{1}{Pe u} \left[\left(\frac{\partial^2 \bar{T}_j}{\partial y^2} \right)_i + \frac{\Delta y^2}{12} \left(\frac{\partial^4 \bar{T}_j}{\partial y^4} \right)_i \right]$$

Here as $\Delta x, \Delta y \rightarrow 0$ we get:

$$\left(\frac{\partial \bar{T}_j}{\partial x}\right)_i = \frac{1}{u} \left(\frac{\partial^2 \bar{T}_j}{\partial y^2}\right)_i \quad (2.111)$$

which is our original PDE, therefore we can conclude that our scheme is consistent.

As being stable and consistent, our scheme is convergent [43].

3. RESULTS AND DISCUSSION

There are a total of eight cases to be studied in this section. These are clear channel, presence of a porous medium, presence of a magnetic field and presence of both porous medium and magnetic field. Each case is studied for Dirichlet and Neumann boundary conditions. The last two cases, which are Dirichlet and Neumann problems of the case with porous medium and magnetic field, are investigated deeper than the others since they are the ultimate goal of the investigation.

Another point here is, of course, the problem of accuracy. As it is stated before there is an analytic solution to (2.56) given as (2.100) which has no viscous dissipation term. When the core error of the core code compared to this analytical solution and Mathematica's integrated numerical differential equation solver [NDSolve] the following results are obtained:

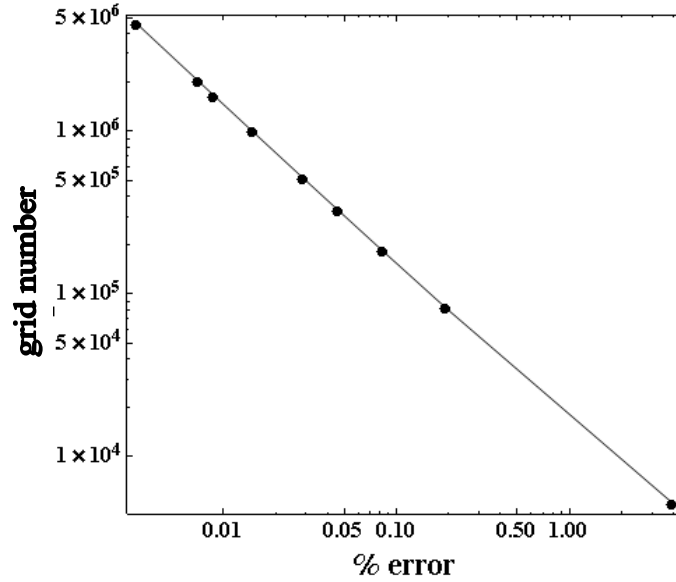


Figure 3.1 : The error dependance on grid number

Mean error between NDSolve and core code is $2.56726 \times 10^{-3} \%$.

Mean error between Analytic solution and NDSolve is $4.88676 \times 10^{-5} \%$.

Mean error between Analytic solution and core code is $3.21078 \times 10^{-3} \%$.

The error dependance on the grid size of the numerical scheme is plotted on Fig. 3.1 above. Due to hardware restrictions the grid no further refined.

As it can be seen here NDSolve gives trustable results and although the errors are very small, NDSolve has a smaller error compared to the core code, which in fact can be refined by increasing the mesh but would require more computing time. Therefore the Dirichlet cases are compared to NDSolve due to the fact that there is no analytical solutions for exactly the same cases as studied here and results are tabulated in Table 3.1:

Table 3.1: Error comparison between NDSolve and the core code for Dirichlet problems

Clear channel	Porous case	Magnetic case	Both porous and magnetic case
$2.45745 \times 10^{-3} \%$	$4.3816 \times 10^{-3} \%$	$4.11922 \times 10^{-3} \%$	$7.25821 \times 10^{-3} \%$

3.1 Clear Channel

In this case there is a viscous, laminar and incompressible flow in a clear channel with viscous dissipation effects included both energy equation and entropy generation equation. The problem geometry is given in Fig. 2.2.

3.1.1 Dirichlet problem

The equation (2.43) is plotted in Fig 3.2 below subjected to the boundary conditions in (2.40). As it can be seen in the figure the maximum velocity occurs in the centre of the channel, whilst it slows down towards to the walls of the channel.

For the Dirichlet problem the equation (2.66) is plotted in Fig. 3.3 subjected to the boundary conditions given as (2.59) and (2.60).

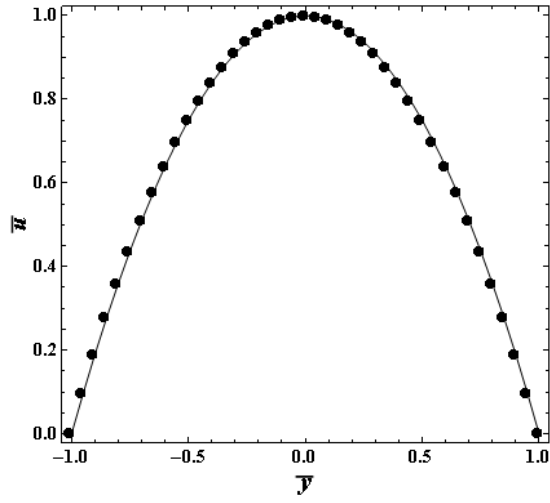


Figure 3.2 : Velocity profile of clear channel

As the fluid advances into the channel its temperature rises until there is no difference between the walls and the fluid due to the fact that the walls are at constant dimensionless temperature and there is no heat generation nor is there another phenomenon the cause heat generation inside the fluid.

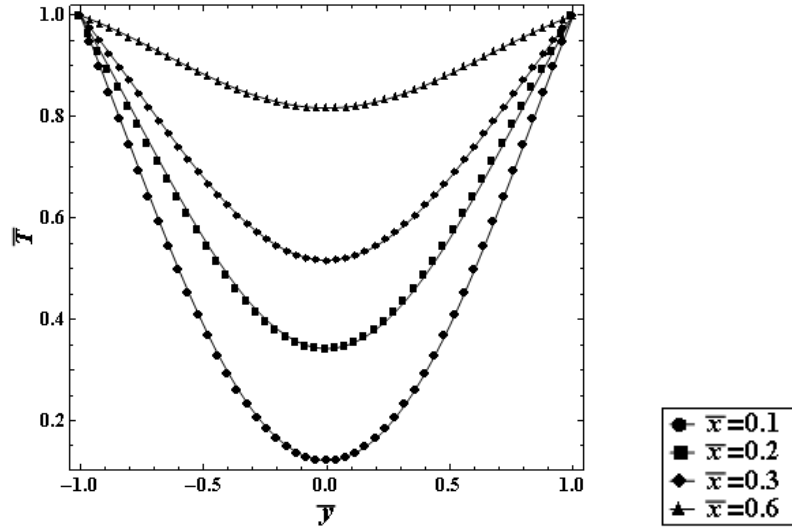


Figure 3.3 : Temperature profile of clear channel for different \bar{x} stations at $Br = 0.1$

Entropy generation is acquired from the solution of (2.88). The Fig. 3.4 shows that entropy generation decreases sharply towards $\bar{y} = 0$ since both thermal and velocity gradients are zero at this point due to the symmetry of the problem.

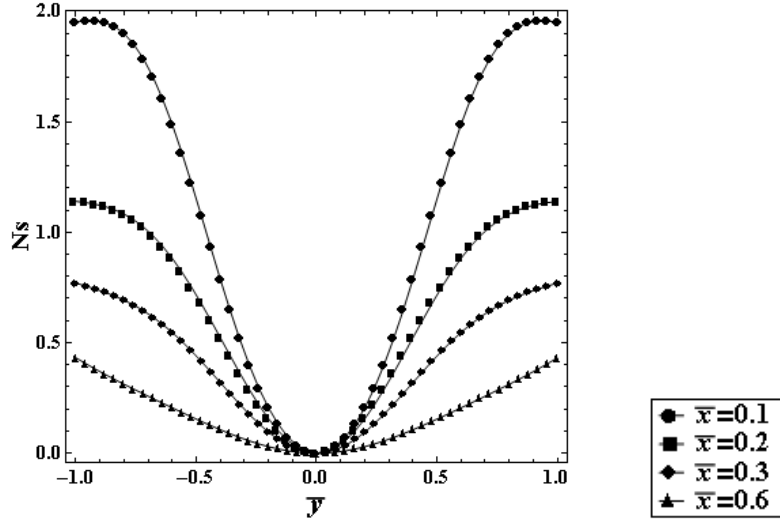


Figure 3.4 : Entropy generation at different \bar{x} stations at $\bar{x} = 0.2$, $Pe = 100$, $Br\Omega^{-1} = 0.1$

Entropy generation becomes significant in the region close to $\bar{y} = \pm 1$ since the wall has a strong effect on entropy generation because of the sudden change of temperature. Notice that entropy generation is dominant near the entrance and decreases towards the further regions of \bar{x} .

Bejan number is obtained from (2.86) and plotted in Fig. 3.5. Figure shows that the irreversibility caused by viscous friction between the walls and the fluid dominates at the walls, especially for high values of dimensionless axial distance; on the other hand, the heat transfer irreversibility dominates towards the centre of the channel.

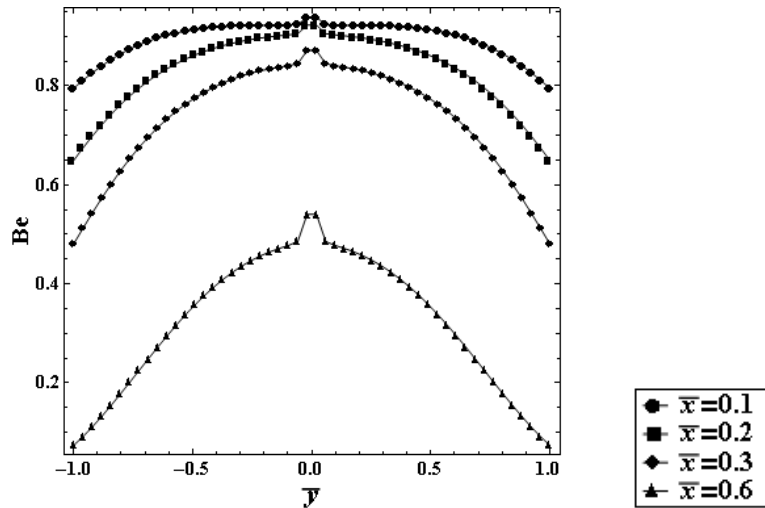


Figure 3.5 : Bejan number at different \bar{x} station at $Pe = 100$, $Br\Omega^{-1} = 0.1$

In the vicinity of the centreline of the channel, namely $\bar{y} = 0$, Bejan number is equal to 1, since the only contribution at this point comes from the gradient of temperature in the \bar{x} direction. The gradients of temperature and velocity in the \bar{y} direction are zero at this point due to the symmetry. Bejan number increases with decreasing \bar{x} , which shows that heat transfer irreversibility is dominant in the entrance region.

3.1.2 Neumann problem

Since the fully developed flow is used for the velocity distribution the profile given in Fig. 3.2 is also valid for this case.

Again the equation (2.65) is plotted in Fig. 3.6. However, due to the fact that there is uniform heat flux conditions, which is given as (2.64) at both of the walls, the temperature of the fluid continues to increase with the increasing \bar{x} .

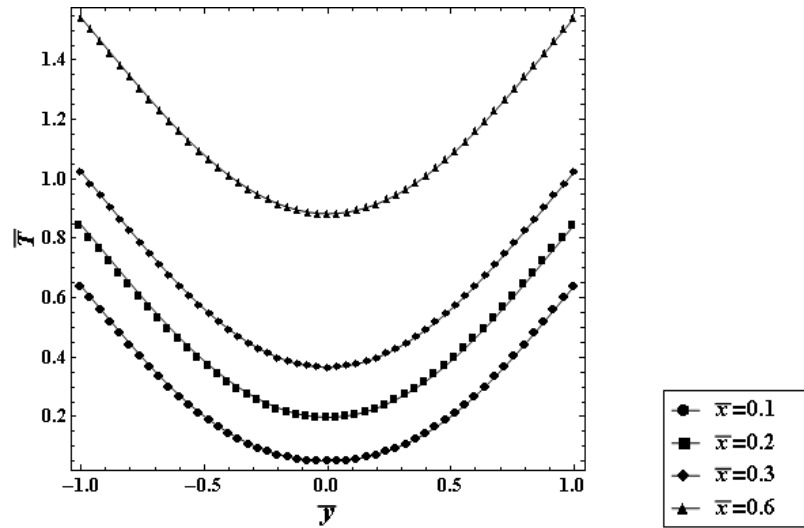


Figure 3.6 : Temperature profile of clear channel for different \bar{x} stations at $Br = 0.1$

The entropy generation in this case occurs very rapidly in the entrance and does not increase very much with the increasing \bar{x} . Again the entropy generation in the vicinity and towards to $\bar{y} = \pm 1$ increases for there is both viscous friction between the wall and the fluid here as well as heat transfer from the wall as seen on Fig. 3.7

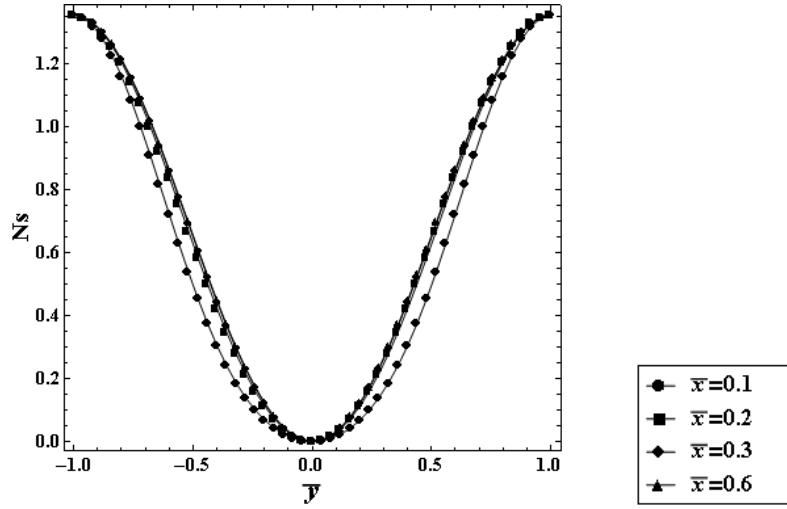


Figure 3.7 : Entropy generation for different \bar{x} profiles at $Pe = 100$, $Br\Omega^{-1} = 0.1$

As it can be seen on Fig. 3.8, despite the fact that entropy generation due to fluid friction gains importance towards $\bar{y} = \pm 1$, the heat transfer irreversibility dominates.

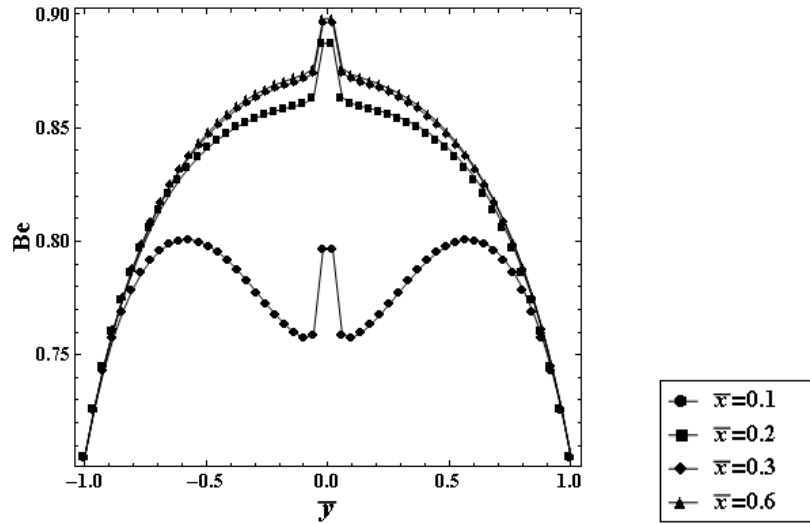


Figure 3.8 : Bejan number for different \bar{x} stations at $Pe = 100$, $Br\Omega^{-1} = 0.1$

The smallest Be is around 0.65 which denotes that the irreversibility favors heat generation.

3.2 Presence of Porous Medium

In this case there is a viscous, laminar and incompressible flow in a channel with a uniform porous medium inside it. The problem geometry is given in Fig. 2.3. Viscous dissipation effects included both energy equation and entropy generation equation.

3.2.1 Dirichlet problem

The equation (2.46) is plotted for different Da numbers in Fig. 3.9. As it can be seen with the decreasing Da numbers, which mean decreasing permeability of the porous medium, the velocities in the channel tends to be decreasing reaching 0 due to the boundary conditions given as (2.40).

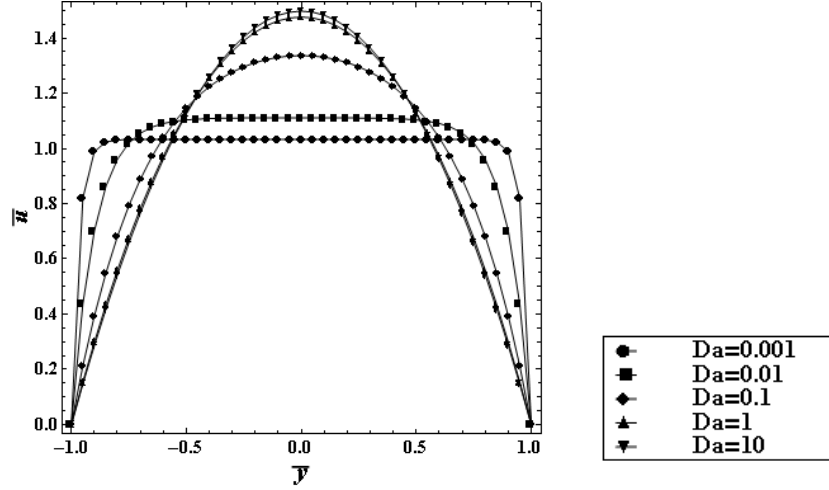


Figure 3.9 : Velocity profiles of the porous case for different Da

The equation (2.68) is plotted in Fig. 3.10. Unlike the temperature distribution of the clear case discussed above as the increasing \bar{x} , the temperatures exceeds that of the walls temperature due to the heat generation caused by viscous effects because of the porous medium.

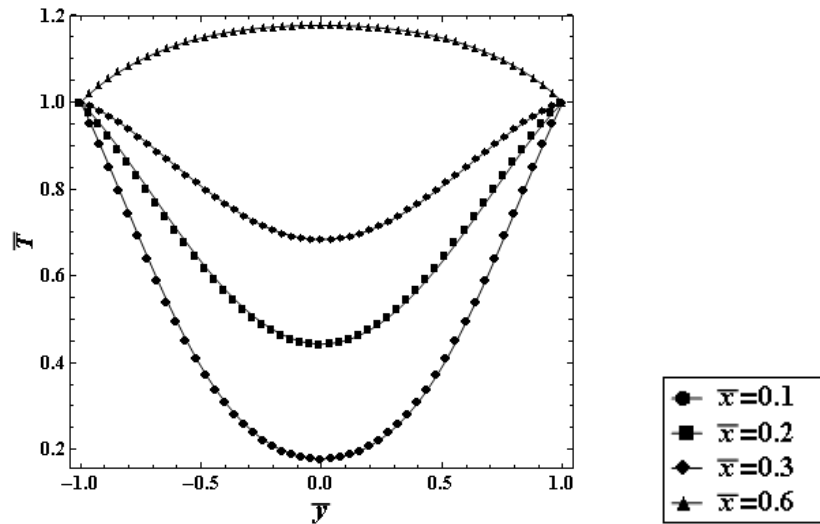


Figure 3.10 : Temperature profiles for different \bar{x} stations at $Br = 0.1$, $Da = 0.1$

The equation (2.91) is plotted in Fig. 3.11. Again the entropy generation is larger at the entrance region of the channel as seen on Fig. 3.11. However, Fig. 3.12 denotes that in this case the fluid friction is the dominant cause of entropy generation because of the porous medium.

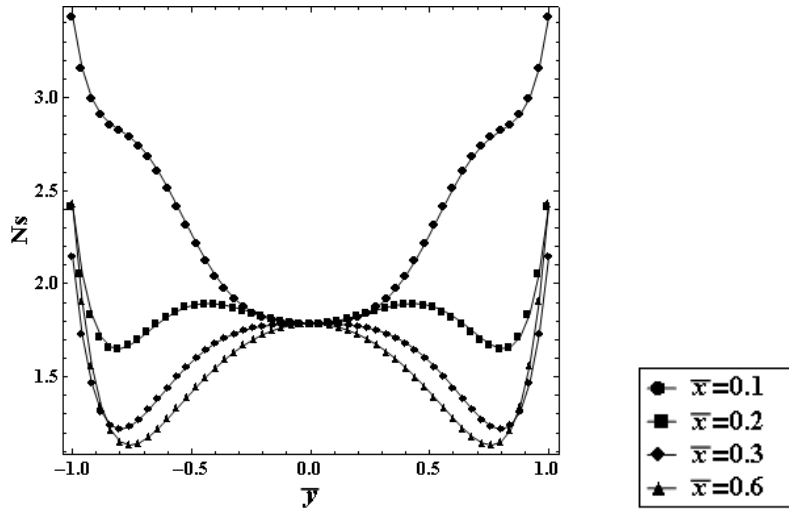


Figure 3.11 : Entropy generation for different \bar{x} stations at $Pe = 100$, $Br\Omega^{-1} = 0.1$, $Da = 0.1$

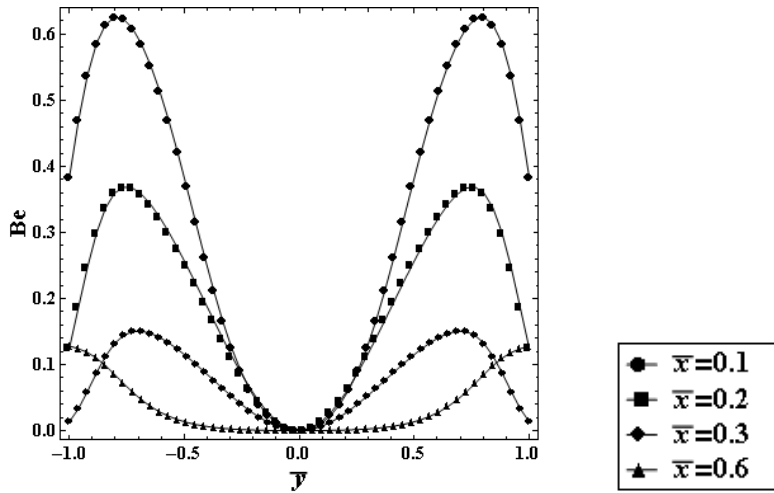


Figure 3.12 : Bejan number for different \bar{x} stations at $Pe = 100$, $Br\Omega^{-1} = 0.1$, $Da = 0.1$

With the increasing \bar{x} the importance of the irreversibility caused by heat transfer decreases.

3.2.2 Neumann problem

Temperature profiles are obtained by solving (2.68) and these distributions are plotted in Fig. 3.13 at different stations of \bar{x} for $Pe = 100$, $Br = 0.1$, $Da = 0.1$.

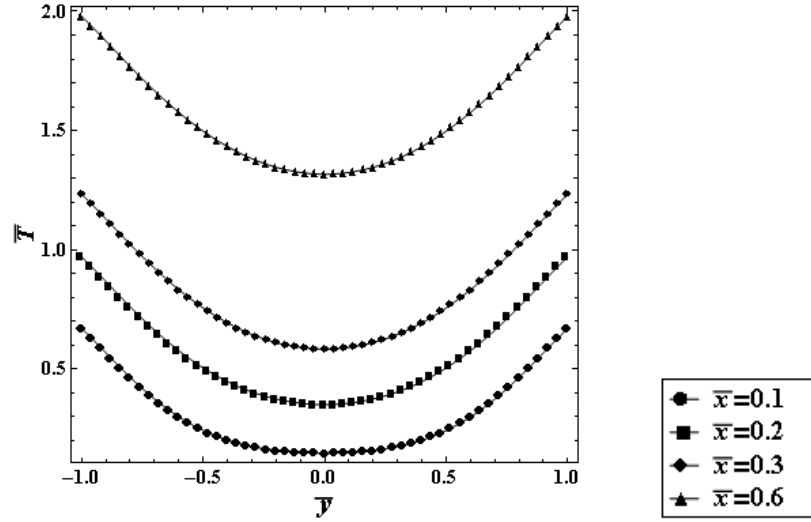


Figure 3.13 : Temperature profiles for different \bar{x} stations at $Br = 0.1$, $Da = 0.1$

It can be seen from the figure, temperature profiles are symmetrical along the $\bar{y} = 0$ axis and the magnitude of temperature increases with increasing \bar{x} as expected.

Entropy generation of this case is obtained from (2.91). Fig 3.14 shows that, far from the entrance section, entropy generation decreases sharply towards $\bar{y} = 0$ line since both thermal and velocity gradients are zero at this point due to the symmetry of the problem. Entropy generation becomes significant in the region close to $\bar{y} = \pm 1$ since the walls have a strong effect on entropy generation because of the sudden change in temperature as well as the flow velocity.

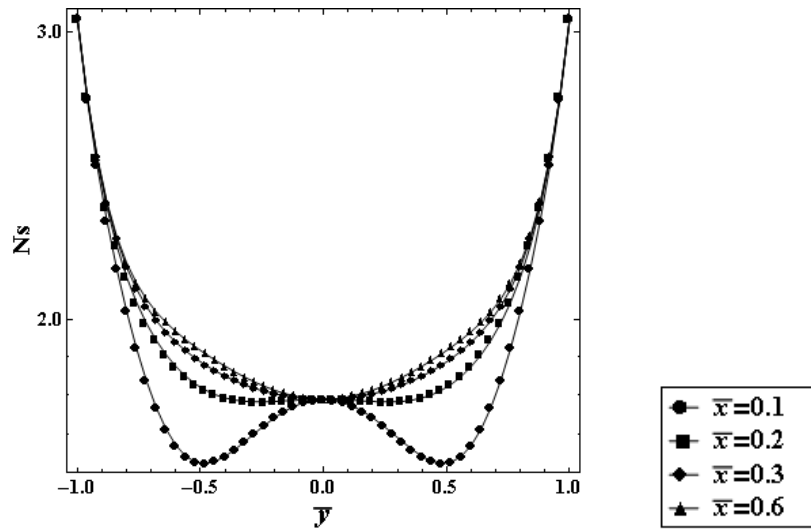


Figure 3.14 : Entropy generation for different \bar{x} stations at $Pe = 100$, $Br\Omega^{-1} = 0.1$, $Da = 0.1$

In this case, again the entropy generation due to fluid friction plays the dominant role as seen on Fig. 3.15, especially towards $\bar{y} = 0$ and relatively in the near regions of the walls or in other words $\bar{y} = \pm 1$.

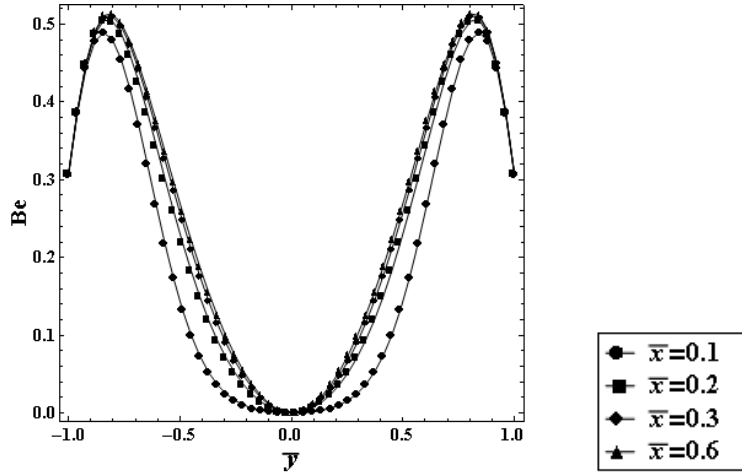


Figure 3.15 : Bejan number for different \bar{x} stations at $Pe = 100$, $Br\Omega^{-1} = 0.1$, $Da = 0.1$

3.3 Presence of Magnetic Field

In this case there is a viscous, laminar and incompressible flow in a channel with a magnetic field acting on it. The problem geometry is given in Fig. 2.4. Viscous dissipation effects included both energy equation and entropy generation equation.

3.3.1 Dirichlet problem

The equation (2.49) is plotted for different Ha numbers in Fig. 3.16. As it can be seen with the decreasing Ha numbers, which mean decreasing permeability of the porous medium, the velocities in the channel tends to be decreasing reaching 0 due to the boundary conditions given as (2.40).

The equation (2.70) is plotted in Fig. 3.17. Unlike the temperature distribution of the clear case discussed above as the increasing \bar{x} , the temperatures exceeds that of the walls temperature due to the heat generation caused by viscous effects because of the magnetic field acting on the fluid very much like as it is in the porous case.

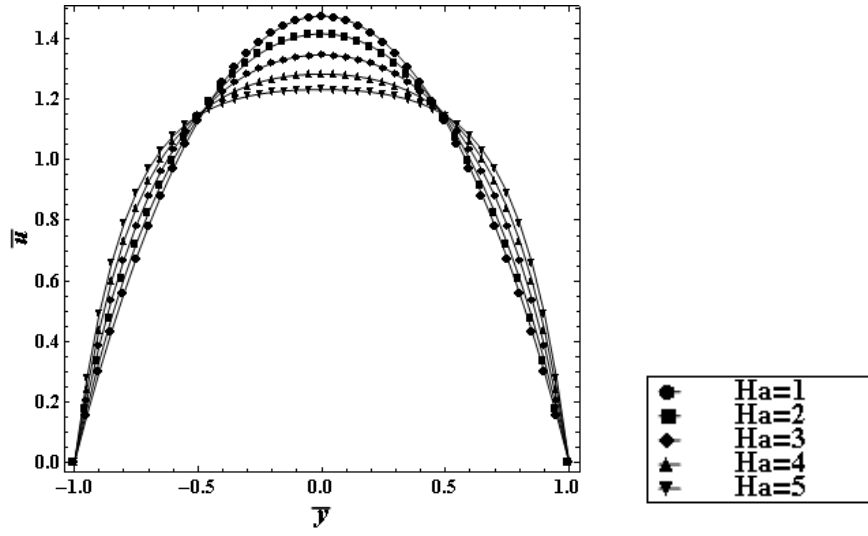


Figure 3.16 : Velocity profiles of the magnetic case at different Ha

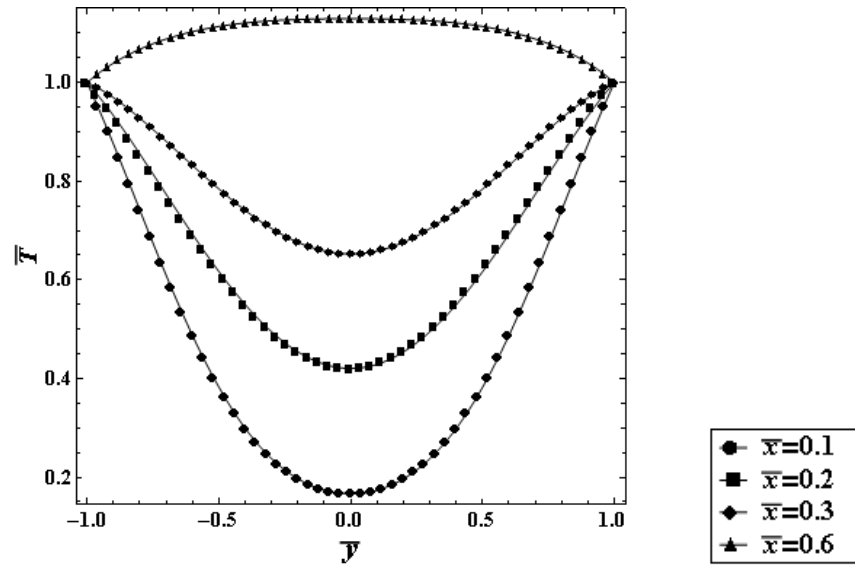


Figure 3.17 : Temperature profiles for different \bar{x} stations at $Br = 0.1$, $Ha = 3$

The magnetic field acting on the fluid behaves very much like the porous medium in terms of entropy generation and the dominant causes of it as it seen on Figs. 3.17 and 3.18. The entropy generation tends to increase towards to $\bar{y} = \pm 1$ and decrease with increasing \bar{x} . However, unlike the clear case discussed above the entropy generation in the centre of the channel is greater due to the magnetic field.

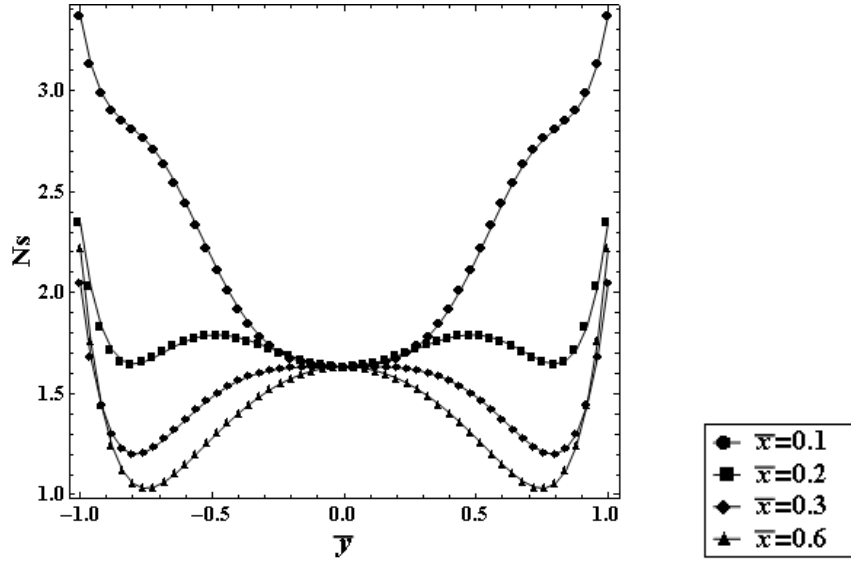


Figure 3.18 : Entropy generation for different \bar{x} stations at $Pe = 100$, $Br\Omega^{-1} = 0.1$, $Ha = 3$

In Fig. 3.19 the Bejan number is plotted at different stations of \bar{x} . As the fluid travels through the channel the irreversibility caused by heat transfer increases, whereas the entropy generation due to fluid friction is dominant near the entrance region.

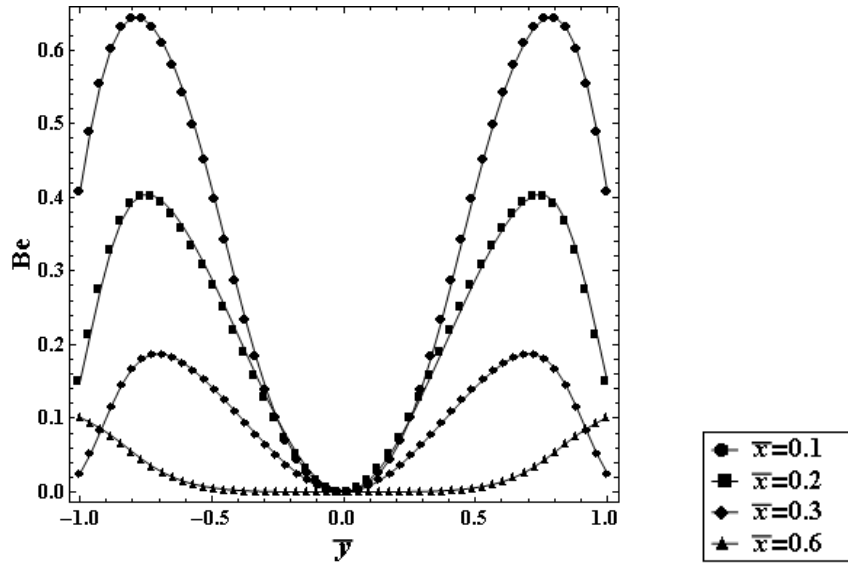


Figure 3.19 : Bejan number for different \bar{x} stations at $Pe = 100$, $Br\Omega^{-1} = 0.1$, $Ha = 3$

3.3.2 Neumann problem

Temperature profiles are obtained by solving (2.70) and these distributions are plotted in Fig. 3.20 at different stations of \bar{x} for $Pe = 100$, $Br = 0.1$, $Ha = 3$.

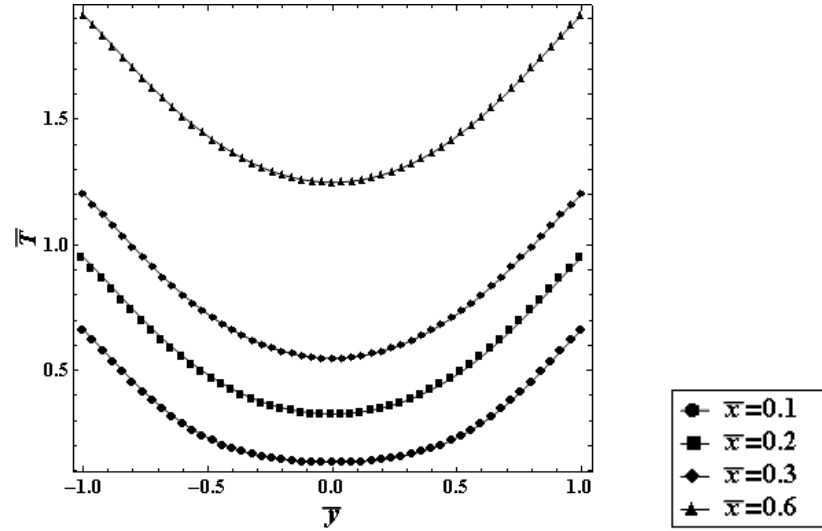


Figure 3.20 : Temperature profiles for different \bar{x} stations at $Pe = 100$, $Br = 0.1$, $Ha = 3$

The equation (2.94) is plotted on Fig. 3.21. As seen on the figure entropy generation tends to increase with increasing \bar{x} . At a given \bar{x} , entropy generation is higher near the walls and quickly decreases towards the centre of the channel, where the irreversibility occurs mostly because of the viscous friction as Fig. 3.22 denotes.

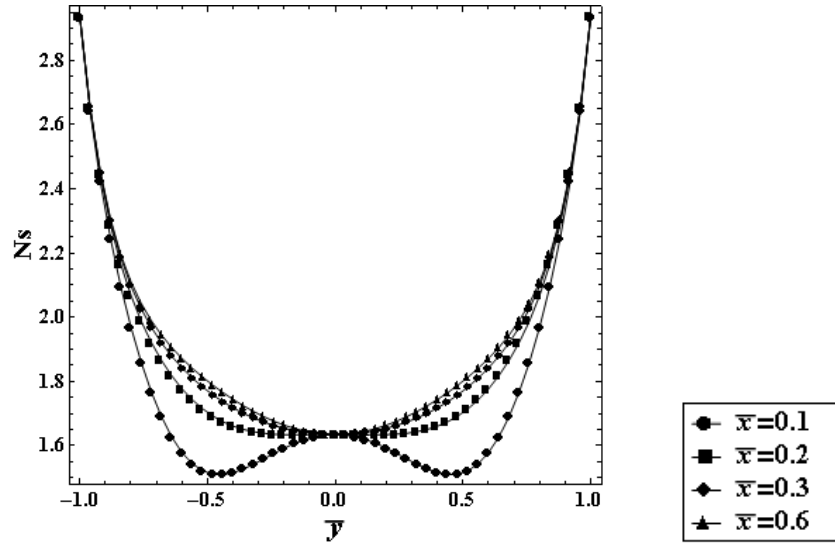


Figure 3.21 : Entropy generation for different \bar{x} stations at $Pe = 100$, $Br\Omega^{-1} = 0.1$, $Ha = 3$

There is a comparison chance of this case with [33], mentioned before, given in (2.101), after a few adjustments to the code. The mean error between the analytical solution here and the code is as low as $1.19332 \times 10^{-15}\%$ and it is presented on Fig. 3.23 below.

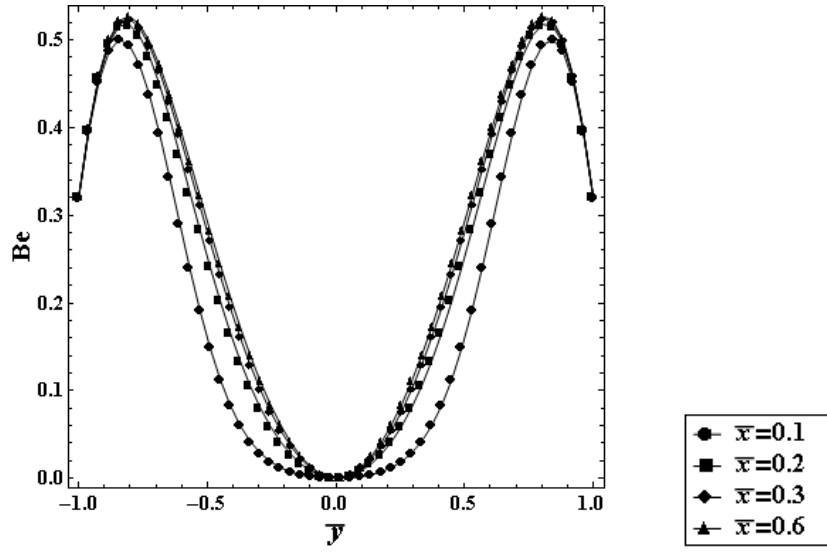


Figure 3.22 : Bejan number for different \bar{x} stations at $Pe = 100$, $Br\Omega^{-1} = 0.1$, $Ha = 3$

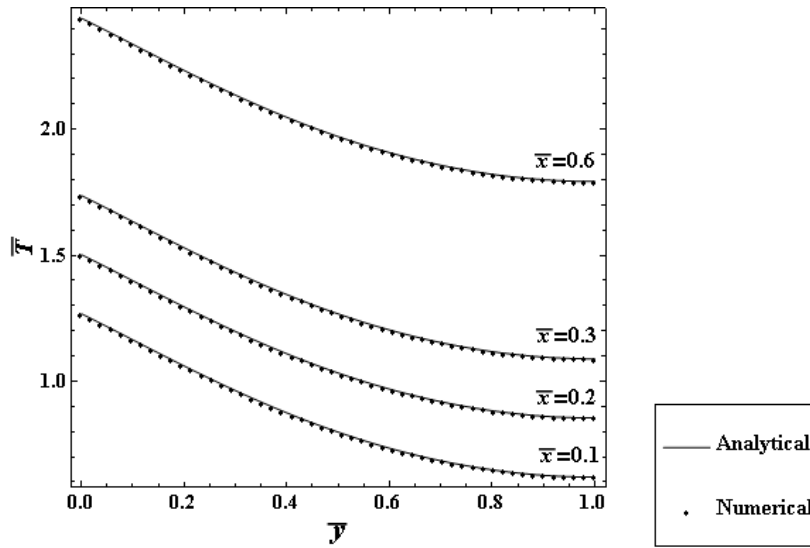


Figure 3.23 : Comparison of analytical and numerical results of magnetic neumann case

3.4 Presence of both Porous Medium and Magnetic Field

3.4.1 Dirichlet problem

The velocity profiles $\bar{u}(\bar{y})$ are presented in Fig. 3.24 for various values of Da . As stated before, an increase in Darcy Number increases the permeability inside the channel, this leads to a non-linear distribution of velocity. Decreasing of the Darcy

number causes to flatten the velocity profile near the centerline region of the channel and slows down the movement of the fluid in the channel.

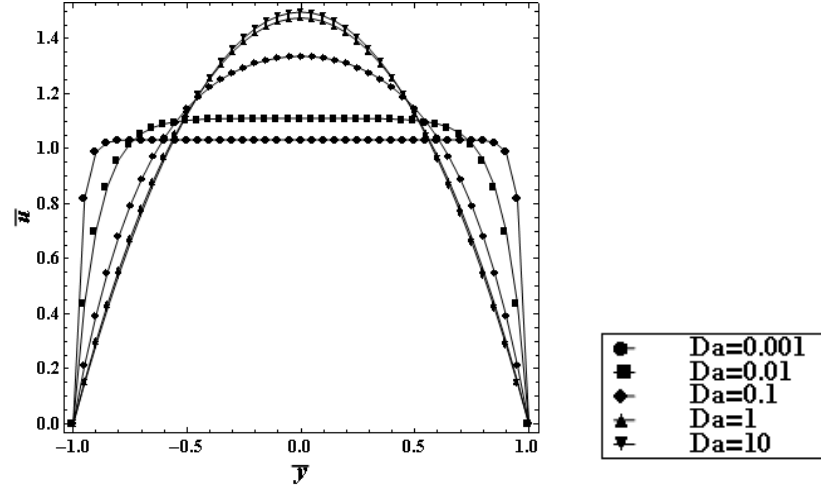


Figure 3.24 : Velocity profile both porous and magnetic case for different Da at $Ha = 3$

The velocity profiles $\bar{u}(\bar{y})$ are plotted in Fig. 3.25 for various values of the Darcy number (Ha). The increasing Ha causes a decrement in velocity especially in the vicinity of the centreline.

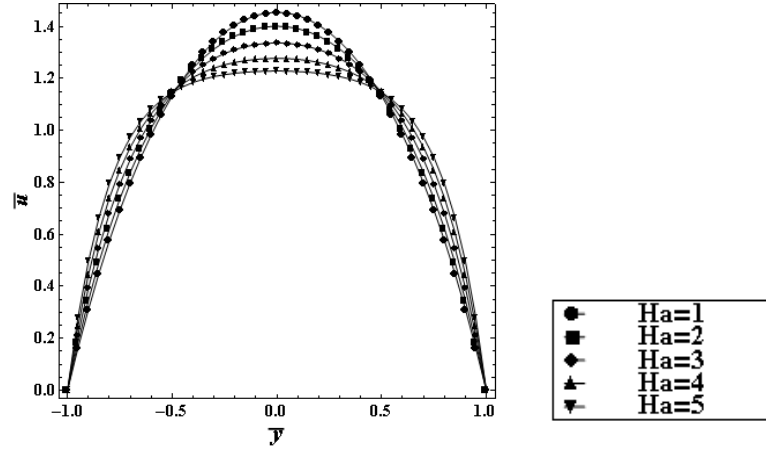


Figure 3.25 : Velocity profile both porous and magnetic case for different Ha at $Da = 0.1$

The temperature profiles for different \bar{x} stations is seen on Fig. 3.26. With the increasing axial distance the temperature of the fluid exceeds the temperature of the wall due to porous and magnetic effects.

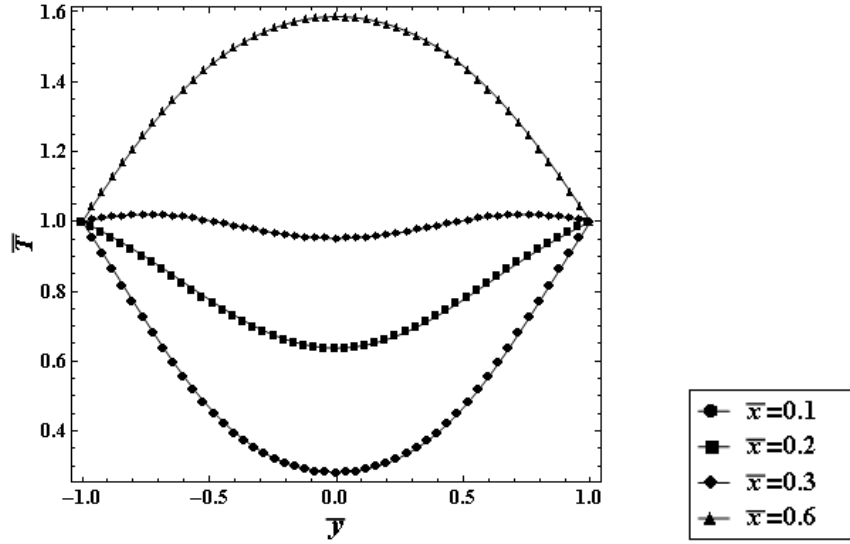


Figure 3.26 : Temperature profiles for different \bar{x} stations at $Pe = 100$, $Br = 0.1$, $Da = 0.1$, $Ha = 3$

Temperature profiles for different Br at $\bar{x} = 0.2$, $Pe = 100$, $Da = 0.1$, $Ha = 3$ is plotted in Fig. 3.27. The increment in the Br causes also the increment of the temperature of the fluid.

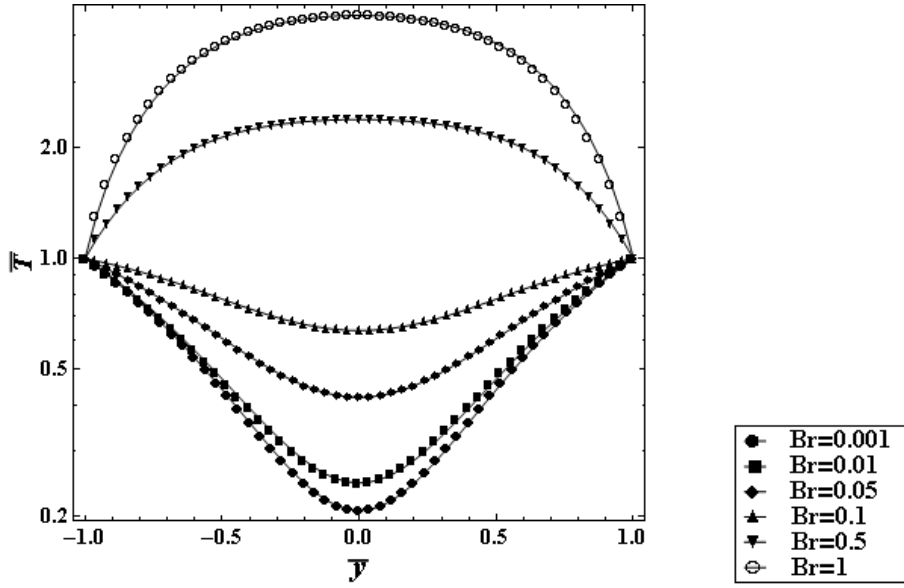


Figure 3.27 : Temperature profiles for different Br at $\bar{x} = 0.2$, $Pe = 100$, $Da = 0.1$, $Ha = 3$

In Fig. 3.28 Temperature profiles for different Da is plotted. It can be seen that as the permeability of the channel decreases, which also mean the decrement of the

Darcy number, the temperature of the fluid increases due to the heat generation caused by the porous effects.

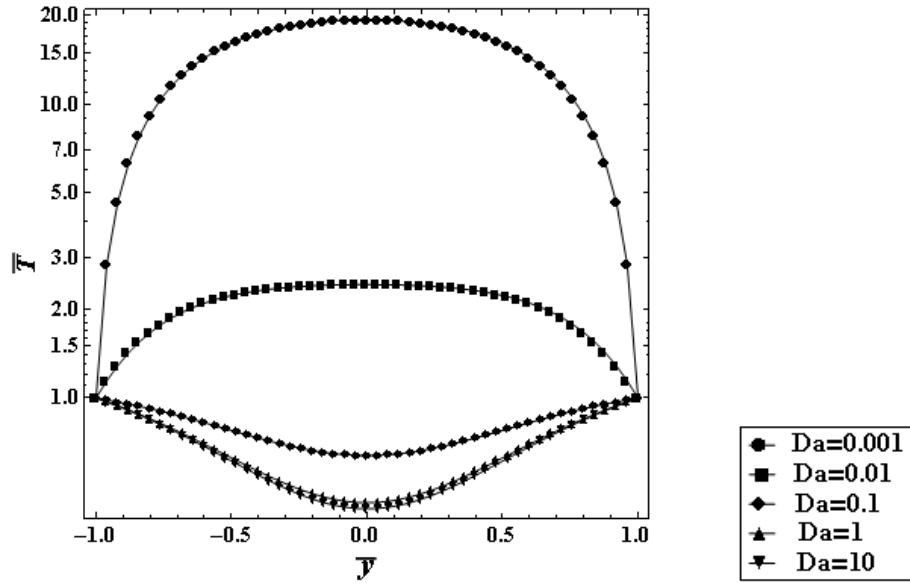


Figure 3.28 : Temperature profiles for different Da at $Pe=100$, $Br=0.1$, $Ha=3$

Like the Darcy number, greater Hartmann numbers increase the temperature of the fluid as seen on Fig. 3.29.

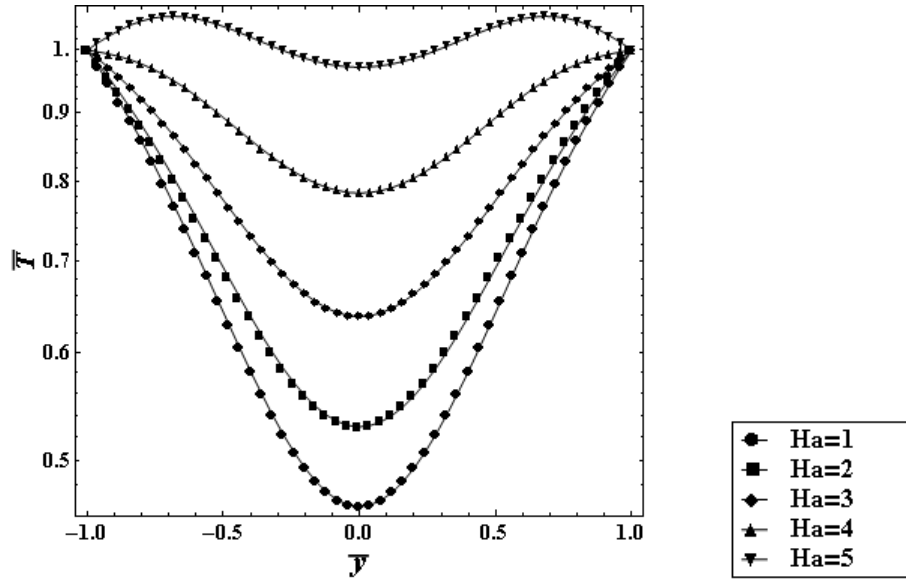


Figure 3.29 : Temperature profiles for different Ha at $Pe=100$, $Br=0.1$, $Da=0.1$

The entropy generation number is seen on Fig. 3.30. The entropy generation is the highest in the entrance. First it tends to decrease for a while as the axial distance increases.

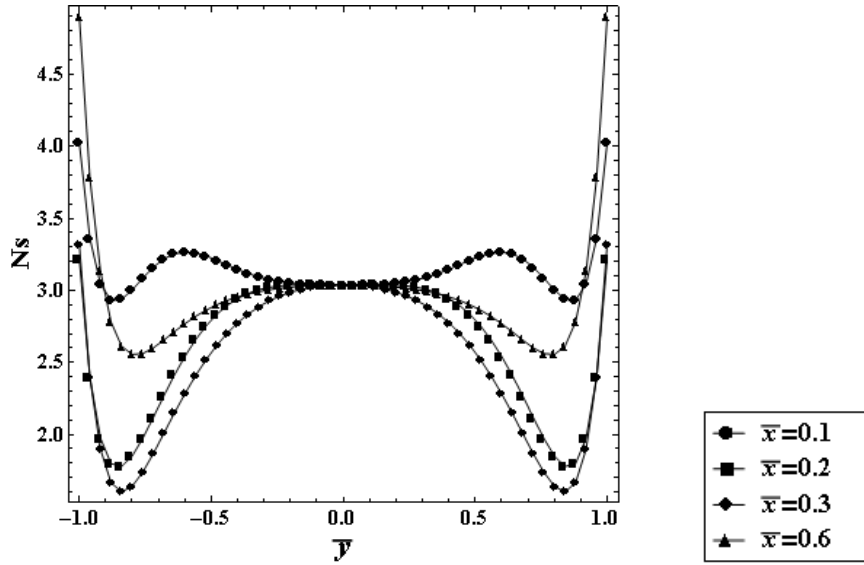


Figure 3.30 : Entropy generation for different \bar{x} stations at $Pe = 100$, $Br\Omega^{-1} = 0.1$, $Da = 0.1$, $Ha = 3$

The small values of Pe increases the entropy generation within the channel, especially in between the $\bar{y} = \pm 0.5$ region of the channel due to the fact that seen on Fig. 3.31 the main reason of the entropy generation in the vicinity of the walls is dominantly fluid friction caused by no slip boundary condition.

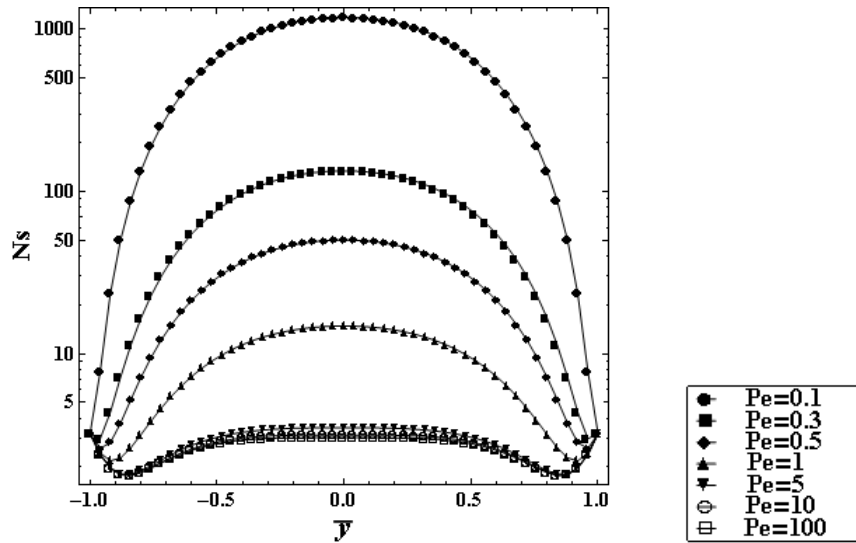


Figure 3.31 : Entropy generation for different Pe at $\bar{x} = 0.2$, $Br\Omega^{-1} = 0.1$, $Da = 0.1$, $Ha = 3$

The increasing Brinkman group parameter increases the entropy generation as it increases entropy generated by viscous dissipation as well as porous and magnetic effects as given in (2.97) and it can be seen on Fig. 3.32.

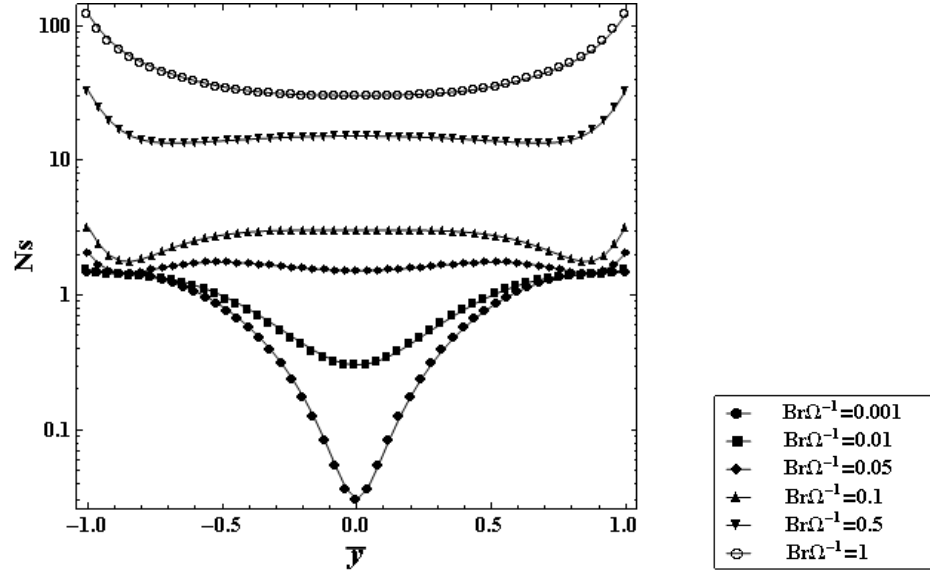


Figure 3.32 : Entropy generation for different $Br\Omega^{-1}$ at $\bar{x} = 0.2$, $Pe = 100$, $Da = 0.1$, $Ha = 3$

In Fig. 3.33 it can be seen that decreasing Darcy number causes a great increment in entropy generation.

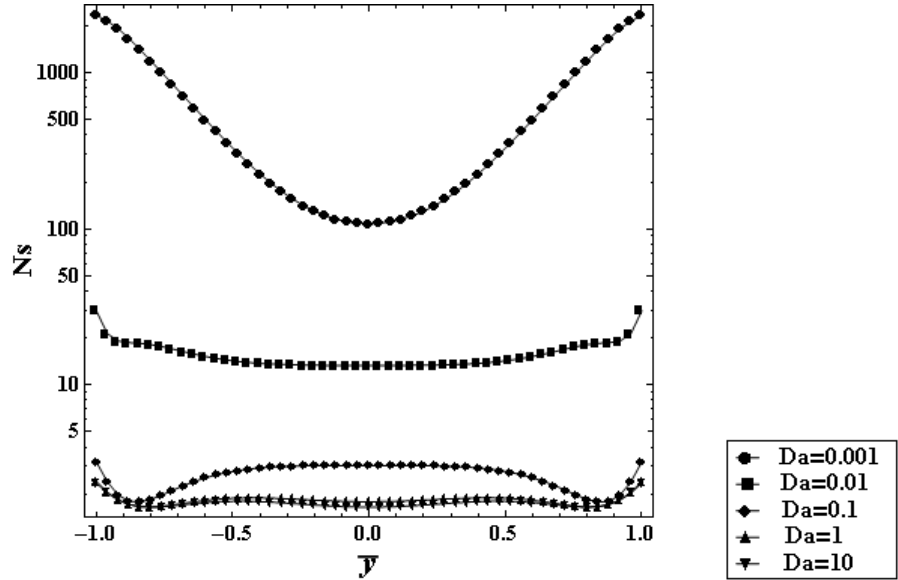


Figure 3.33 : Entropy generation for different Da at $\bar{x} = 0.2$, $Pe = 100$, $Br\Omega^{-1} = 0.1$, $Ha = 3$

The increasing Hartmann number causes the increment of the entropy generation especially that of the centre of the channel as seen on Fig. 3.34.

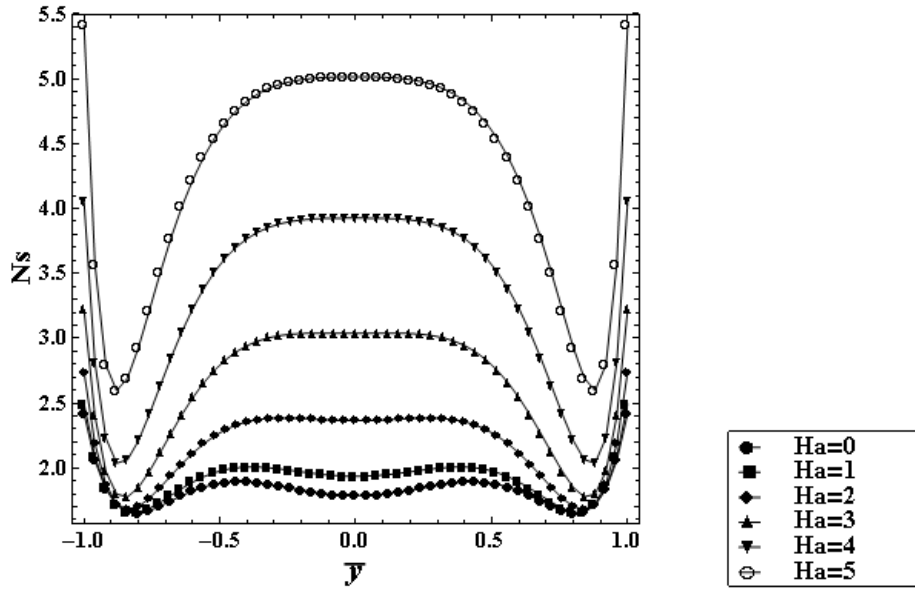


Figure 3.34 : Entropy generation for different Ha at $\bar{x} = 0.2$, $Pe = 100$, $Br\Omega^{-1} = 0.1$, $Da = 0.1$

In this case, as it seen on Fig. 3.35, the main cause of entropy generation is heat transfer near the entrance region. After $\bar{x} = 0.3$ the heat transfer irreversibility gains importance again due to the entrance effects.

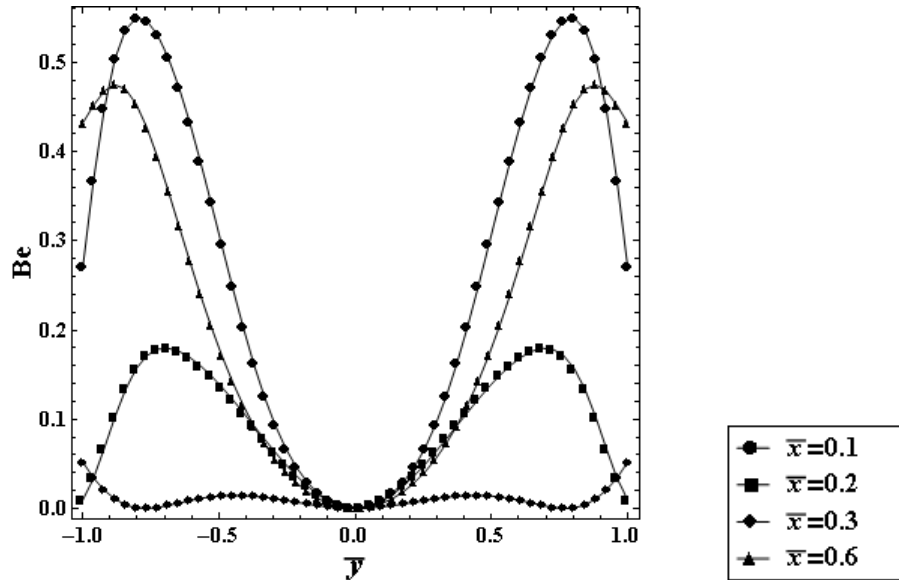


Figure 3.35 : Bejan number for different \bar{x} stations at $Pe = 100$, $Br\Omega^{-1} = 0.1$, $Da = 0.1$, $Ha = 3$

The increasing Pe causes entropy generation due to heat transfer to lose the relative importance against the entropy generation caused by fluid friction, porous and magnetic effects for it is related to the velocity of the fluid as seen on Fig. 3.36.

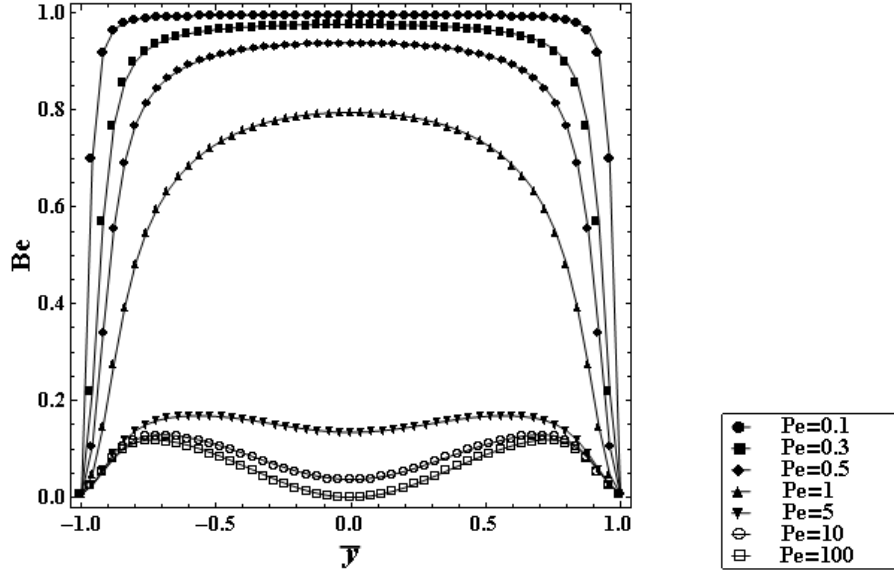


Figure 3.36 : Bejan number for different Pe at $\bar{x} = 0.2$, $Br\Omega^{-1} = 0.1$, $Da = 0.1$, $Ha = 3$

The effect of the group parameter ($Br\Omega^{-1}$) on Bejan number is presented in Fig. 3.37 for $\bar{x} = 0.2$, $Pe = 100$, $Da = 0.1$, $Ha = 3$. An increase in the Brinkman group parameter causes a decrease in Bejan number since the portion of entropy generation caused by the fluid friction irreversibility decreases.

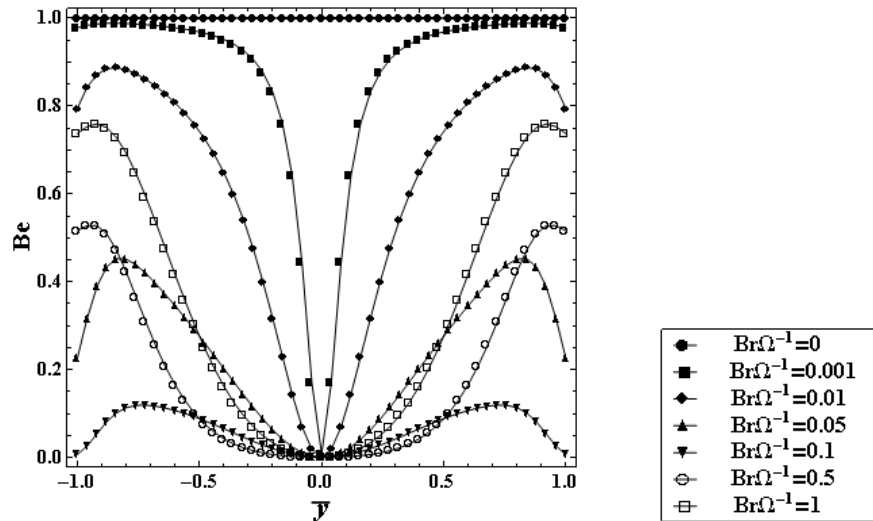


Figure 3.37 : Bejan number for different $Br\Omega^{-1}$ at $\bar{x} = 0.2$, $Pe = 100$, $Da = 0.1$, $Ha = 3$

For $Br\Omega^{-1} = 0$ there is no contribution of viscous dissipation to the irreversibility. In this case heat transfer irreversibility dominates ($Be = 1$). For smaller values of group parameter Bejan number has larger values near the wall decreasing to a minimum value at $\bar{y} = 0$, the temperature gradients are almost zero where there is almost no heat transfer contribution to the irreversibility.

Darcy number affects Bejan number as shown in Fig. 3.38. The increment of Darcy number causes an increment the fluid friction irreversibility, especially in the centre of the channel Bejan numbers approach to the minimum value for here the fluid friction dominates.

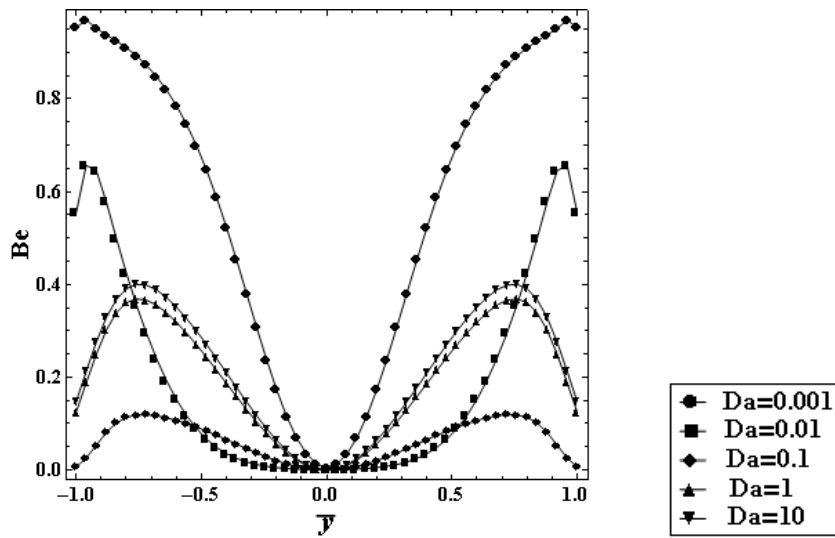


Figure 3.38 : Bejan number for different Da at $\bar{x} = 0.2$, $Pe = 100$, $Br\Omega^{-1} = 0.1$, $Ha = 3$

As seen on Fig. 3.39, the increasing Ha causes the entropy generation due to heat transfer to lose its relative importance.

In Fig. 3.40 the different causes of entropy generation is plotted separately. As it can be seen in the vicinity of the walls the main cause of the irreversibility is fluid friction due to no slip condition. The reason of entropy generation in the vicinity of the centre region is magnetic effects and heat transfer. The entropy generation due to porous medium is relatively low for $Da = 0.1$

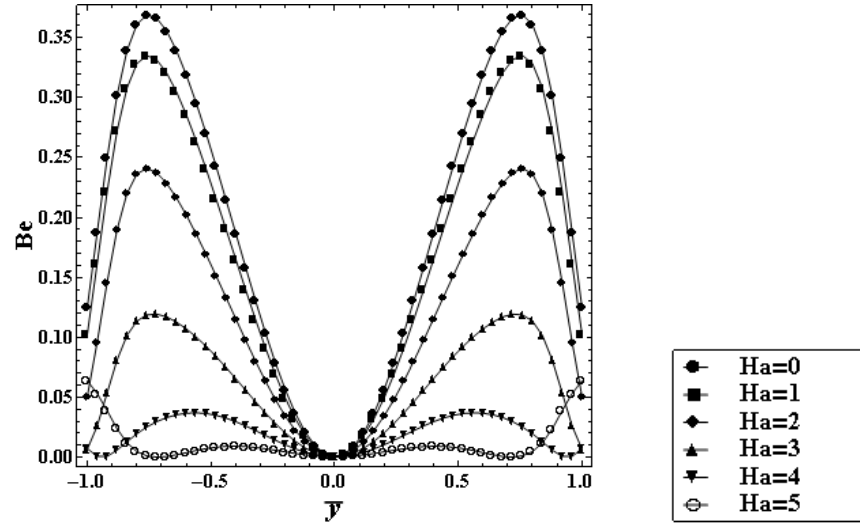


Figure 3.39 : Bejan number for different Ha at $\bar{x} = 0.2$, $Pe = 100$, $Br\Omega^{-1} = 0.1$, $Da = 0.1$

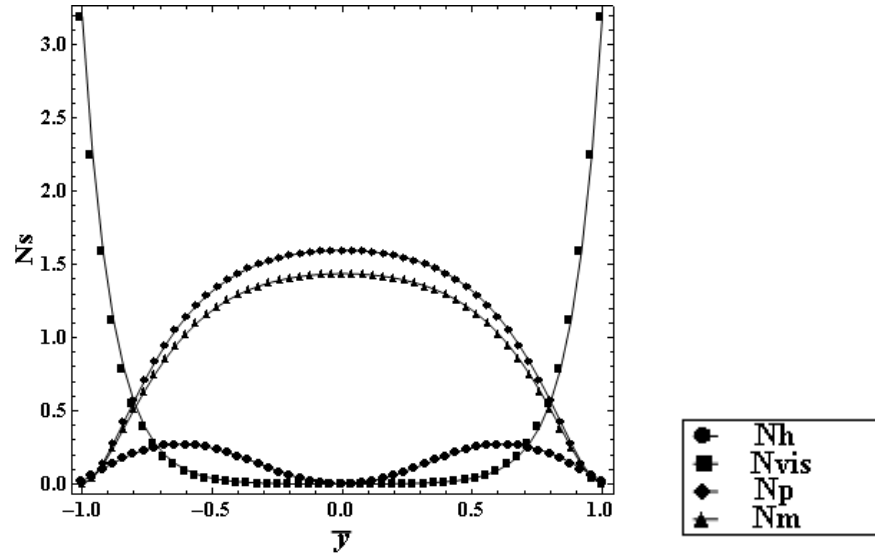


Figure 3.40 : Parts of entropy generation at $\bar{x} = 0.2$, $Pe = 100$, $Br\Omega^{-1} = 0.1$, $Da = 0.1$, $Ha = 3$

For this case, the viscous dissipation term in energy equation given in (2.72) does not cause a great difference in the results of the temperature and entropy generation distribution as seen on Figs. 3.41 and 3.42.

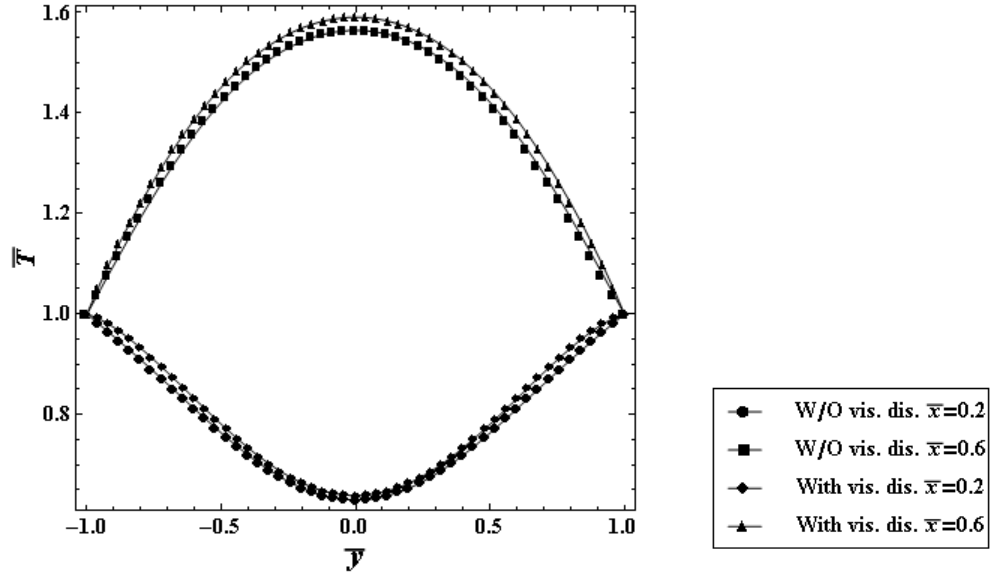


Figure 3.41 : Effect of viscous dissipation on temperature profiles at $Pe = 100$, $Br = 0.1$, $Da = 0.1$, $Ha = 3$

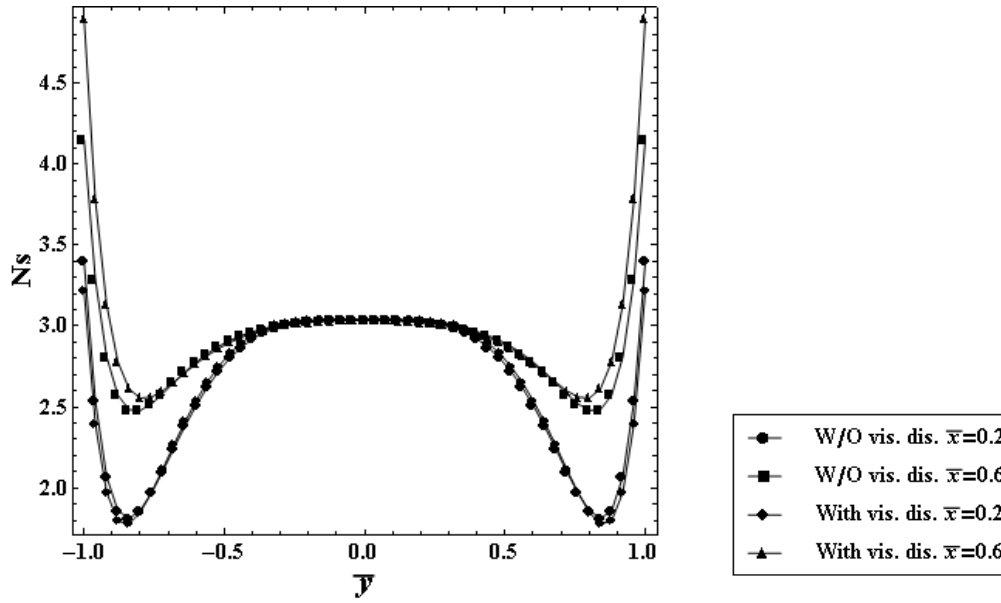


Figure 3.42 : Effect of viscous dissipation on entropy generation at $Pe = 100$, $Br\Omega^{-1} = 0.1$, $Da = 0.1$, $Ha = 3$

3.4.2 Neumann problem

As seen on Fig. 3.43 as the \bar{x} increases the temperature of the fluid increases symmetrically along the channel.

The temperature profiles are shown in Fig. 3.44 for various values of the Brinkman number (Br).

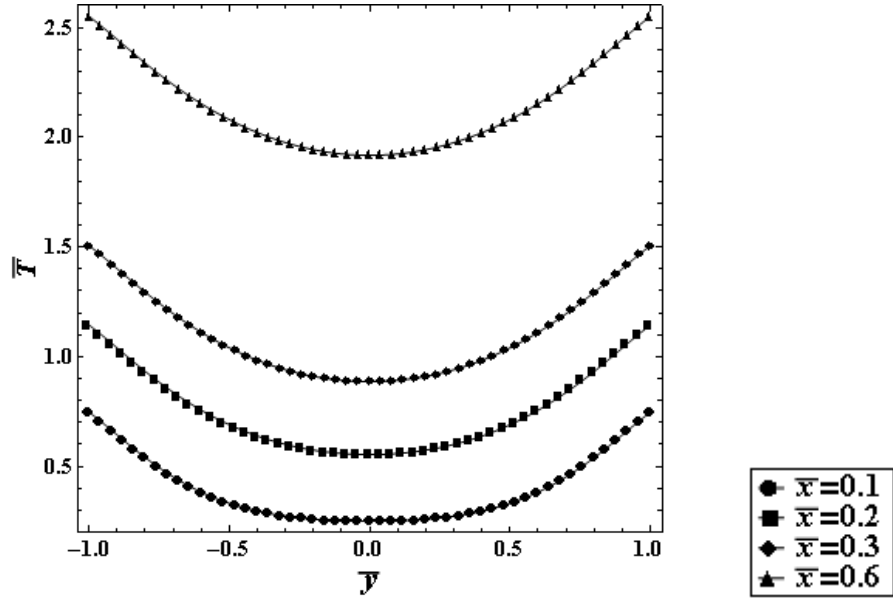


Figure 3.43 : Temperature profiles for different \bar{x} stations at $Pe = 100$, $Br = 0.1$, $Da = 0.1$, $Ha = 3$

With increasing Br number, the magnitude of temperature increases while the difference between the temperature at the centerline of the channel and the temperature at the walls decreases.

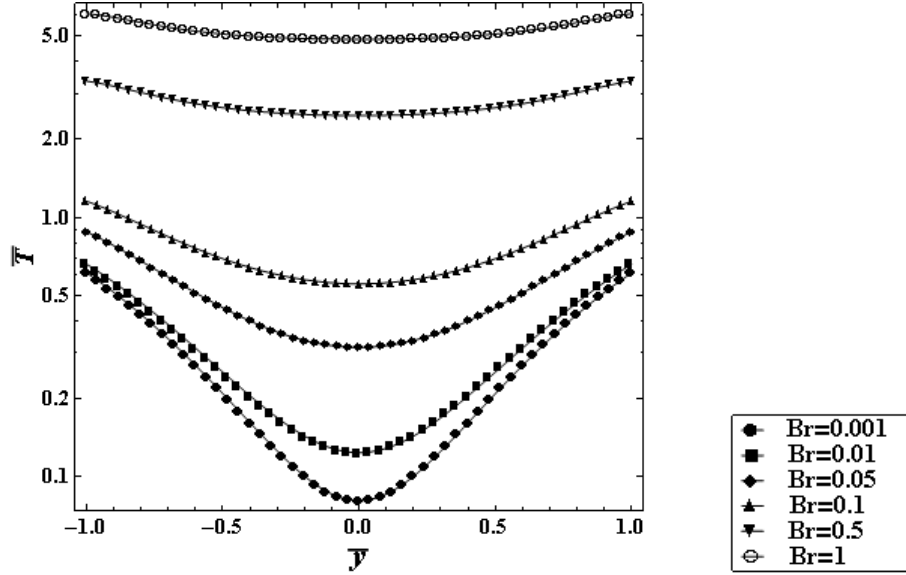


Figure 3.44 : Temperature profiles for different Br at $\bar{x} = 0.2$, $Pe = 100$, $Da = 0.1$, $Ha = 3$

The effect of the Da number on temperature profiles is presented in Fig. 3.45 for $Pe = 100$, $\bar{x} = 0.2$, $Br = 0.1$ and $Ha = 3$. Increasing Da number causes a increment on temperature since the decrement in the value of Da number slows down the

movement of the fluid in the channel and heat dissipation due to the effect of the porosity.

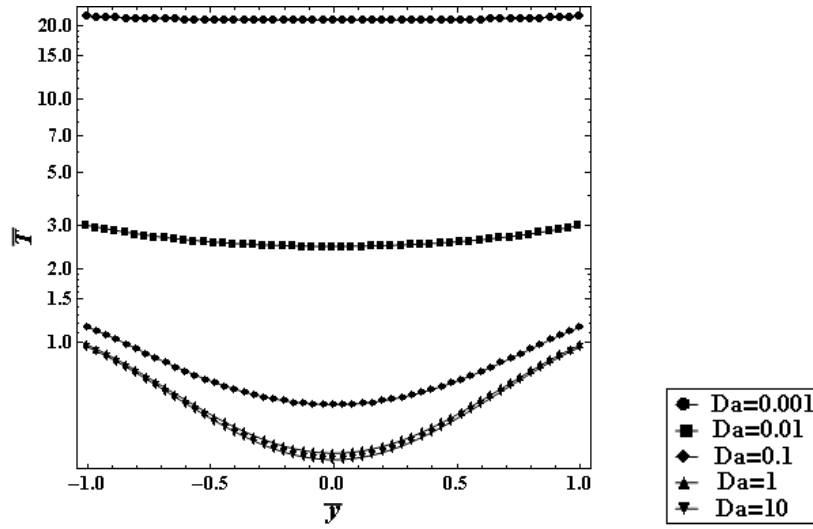


Figure 3.45 : Temperature profiles for different Da at $Pe = 100$, $Br = 0.1$, $Ha = 3$

The effect of Ha on temperature profiles is plotted in Fig. 3.46. As it can be seen in the figure that the increasing Ha numbers causes the temperature throughout the channel to increase.

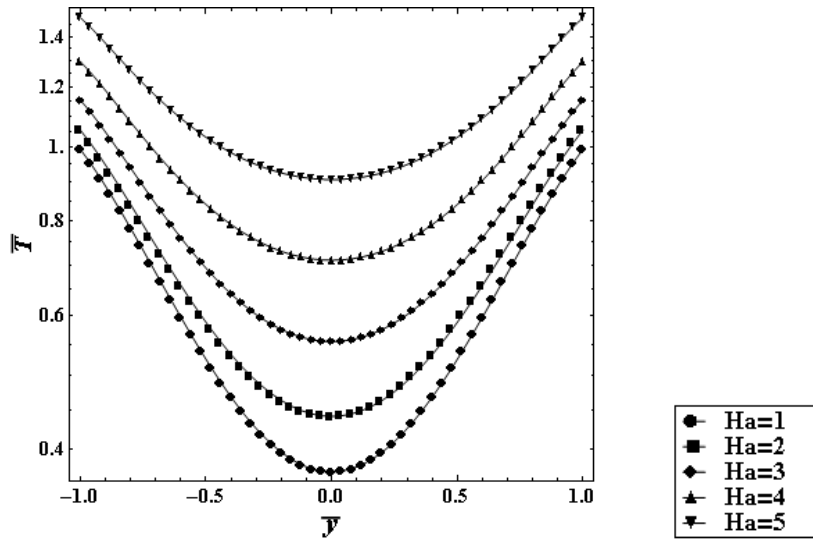


Figure 3.46 : Temperature profiles for different Ha at $Pe = 100$, $Br = 0.1$, $Da = 0.1$

Entropy generation is graphically presented in Fig. 3.47 for $Br\Omega^{-1} = 0.1$, $Da = 0.1$ and $Pe = 100$ at different \bar{x} locations. The figure shows that, far from the entrance section, entropy generation decreases sharply towards $\bar{y} = 0$ line since both thermal

and velocity gradients are zero on this line due to the symmetry of the problem. Entropy generation becomes significant in the region close to $\bar{y} = \pm 1$ since the walls have a strong effect on entropy generation because of the sudden change in temperature as well as the flow velocity.

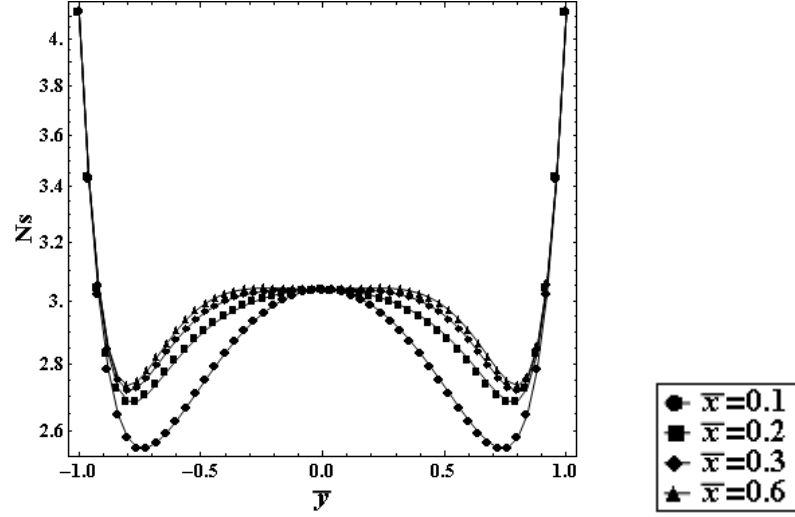


Figure 3.47 : Entropy generation for different \bar{x} stations at $Pe = 100$, $Br\Omega^{-1} = 0.1$, $Da = 0.1$, $Ha = 3$

The assumption of no slip on the walls causes stronger velocity gradients take place close to the walls. This region is the powerful entropy generator and dominates on the total entropy generation.

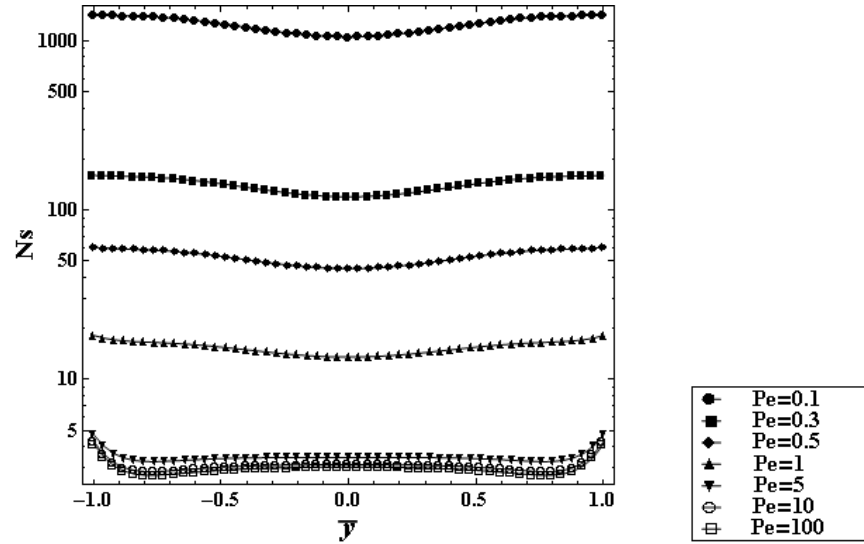


Figure 3.48 : Entropy generation for different Pe at $\bar{x} = 0.2$, $Br\Omega^{-1} = 0.1$, $Da = 0.1$, $Ha = 3$

The local entropy generation number is presented in Fig.3.48 at different values of the Pe number for $Br\Omega^{-1}=0.1, Da=0.1$. Fig. 3.49 shows that the entropy generation number is changing almost linearly in logarithmic scale for different values of Pe number.

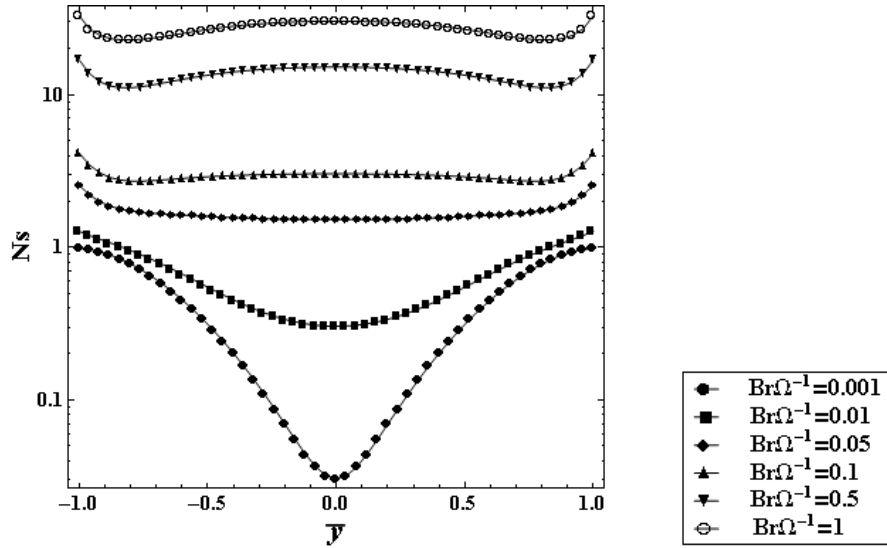


Figure 3.49 : Entropy generation for different $Br\Omega^{-1}$ at $\bar{x} = 0.2$, $Pe = 100$, $Da = 0.1$, $Ha = 3$

The entropy generation number is presented in Fig. 3.49 at different values of the group parameter $Br\Omega^{-1}$ for $\bar{x} = 0.2$, $Pe = 100$, $Da = 0.1$. The group parameter has a strong effect on entropy generation, it also determines the relative importance of the viscous effect. The increase of $Br\Omega^{-1}$ increases the entropy generation number since fluid friction is directly related with this parameter.

The effect of the Da number on entropy generation is presented in Fig. 3.50 for $\bar{x} = 0.2$, $Pe = 1$, $Br\Omega^{-1} = 0.1$. As the Da number increases, which means the permeability of the channel increases for a constant height, the entropy generation number decreases and a minimum entropy generation appears at the centreline of the channel. At the centreline of the channel velocity takes its maximum value and temperature has its minimum value. Because of the symmetry of both fields have zero gradients as a consequence of this they have no contribution to the entropy-generation number.

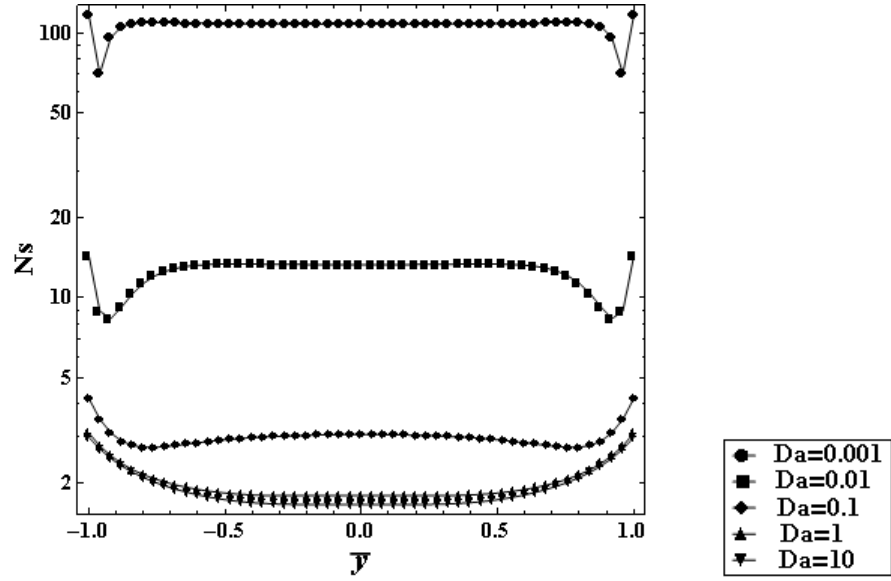


Figure 3.50 : Entropy generation for different Da at $\bar{x} = 0.2$, $Pe = 100$, $Br\Omega^{-1} = 0.1$, $Ha = 3$

In Fig. 3.51, entropy generation for different Ha is plotted. As seen on the figure the higher Ha numbers increase the entropy generation, and after approximately around $Ha = 3$, the effect of magnetic field begins to affect to the centre of the channel at a higher rate.

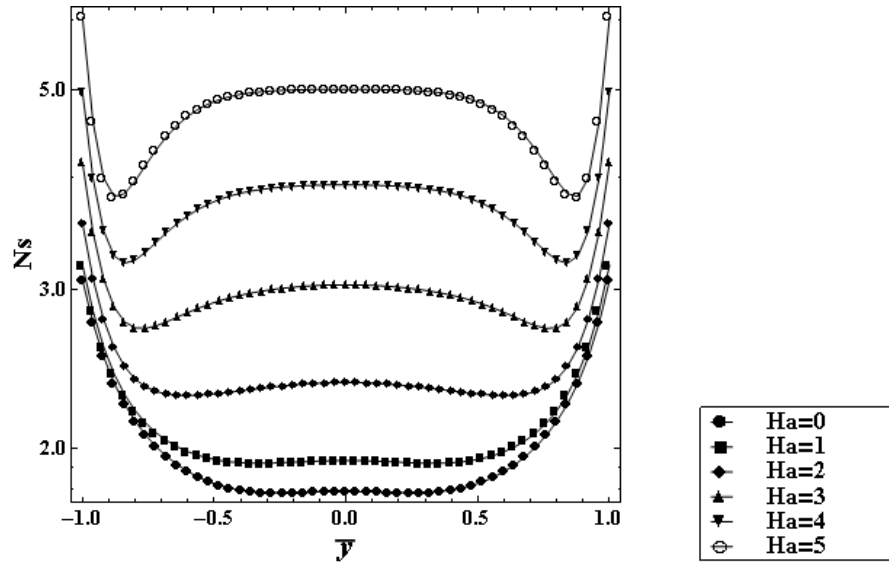


Figure 3.51 : Entropy generation for different Ha at $\bar{x} = 0.2$, $Pe = 100$, $Br\Omega^{-1} = 0.1$, $Da = 0.1$

To have a better understanding of the dominance of the mechanisms which cause entropy generation Be numbers should be studied. Bejan number is obtained from

(2.98) and plotted in Fig. 3.52 at different \bar{x} stations. Fig. 3.52 shows that the irreversibility caused by viscous friction between the walls and the fluid dominates.

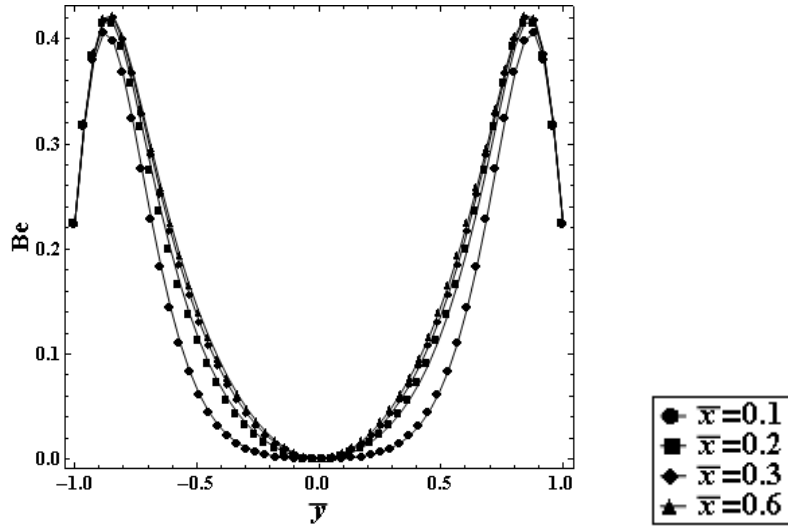


Figure 3.52 : Bejan number for different \bar{x} stations at $Pe = 100$, $Br\Omega^{-1} = 0.1$, $Da = 0.1$, $Ha = 3$

The gradients of temperature and velocity in \bar{y} direction are zero at the centreline of the channel, namely $\bar{y} = 0$, due to the symmetry. Bejan number decreases with decreasing \bar{x} , which shows that heat transfer irreversibility is dominant in the entrance region.

Fig. 3.53 shows the Bejan number for various values of Pe number at $\bar{x} = 0.2$, $Pe = 100$, $Br\Omega^{-1} = 0.1$, $Da = 0.1$, $Ha = 3$. Be number is equal to 1 for small value of Pe number ($Pe = 0.1$) since the only contribution at this point comes from the gradient of temperature in the \bar{x} direction.

The effect of the group parameter ($Br\Omega^{-1}$) on Bejan number is presented in Fig. 3.54 for $\bar{x} = 0.2$, $Pe = 100$, $Da = 0.1$, $Ha = 3$. An increase in the group parameter causes a decrease in Bejan number since the portion of entropy generation caused by the fluid friction irreversibility decreases.

For $Br\Omega^{-1} = 0$ there is no contribution of viscous dissipation to the irreversibility. In this case heat transfer irreversibility dominates ($Be = 1$). For smaller values of group parameter Bejan number has smaller values near the wall, first increases then decreases to a minimum value at $\bar{y} = 0$, the temperature gradients are almost zero. There is no heat transfer contribution to the irreversibility.

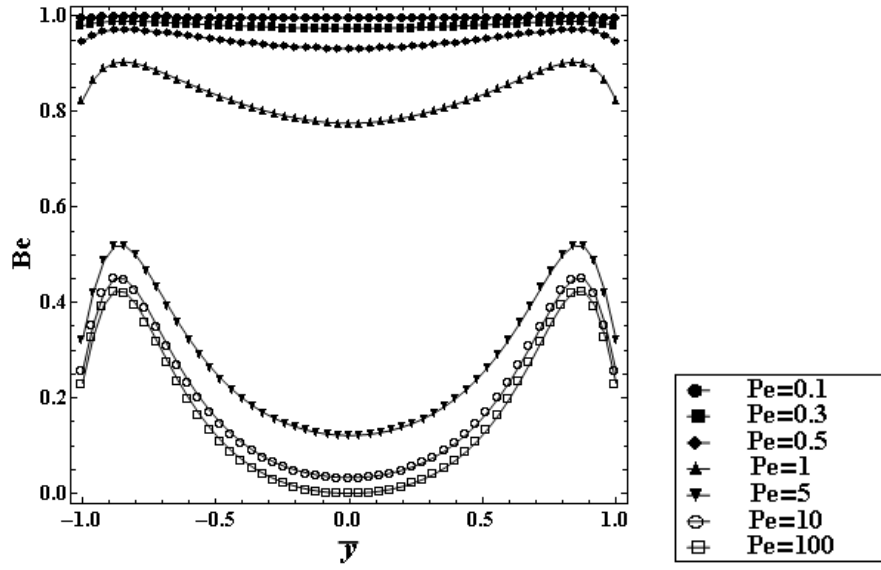


Figure 3.53 : Bejan number for different Pe at $\bar{x} = 0.2$, $Br\Omega^{-1} = 0.1$, $Da = 0.1$, $Ha = 3$

Darcy number affects Bejan number as shown in Fig. 3.55. An increase in Darcy number strengthens the fluid friction irreversibility. Therefore in the centre of the channel Bejan numbers approach to the minimum value, where the fluid friction dominates.

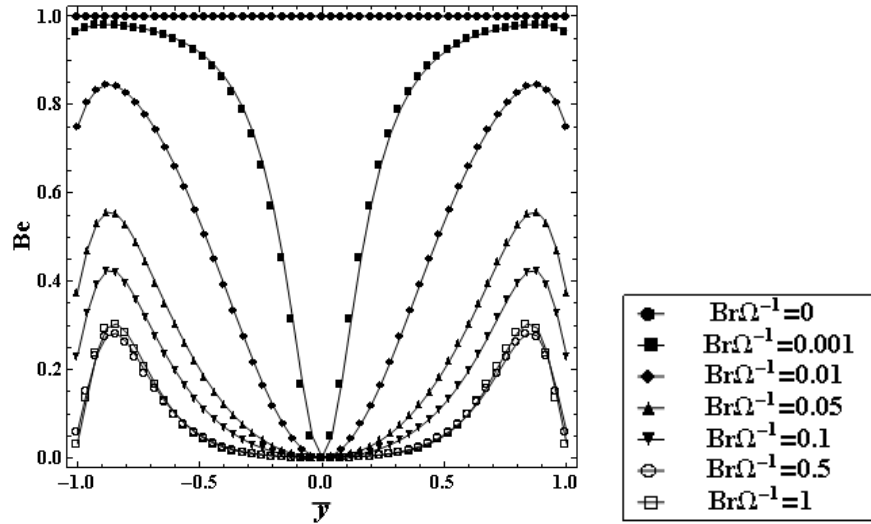


Figure 3.54 : Bejan number for different $Br\Omega^{-1}$ at $\bar{x} = 0.2$, $Pe = 100$, $Da = 0.1$, $Ha = 3$

The Bejan number for different Ha for $Pe = 100$, $Br\Omega^{-1} = 0.1$, $Da = 0.1$ is seen on Fig. 3.56.

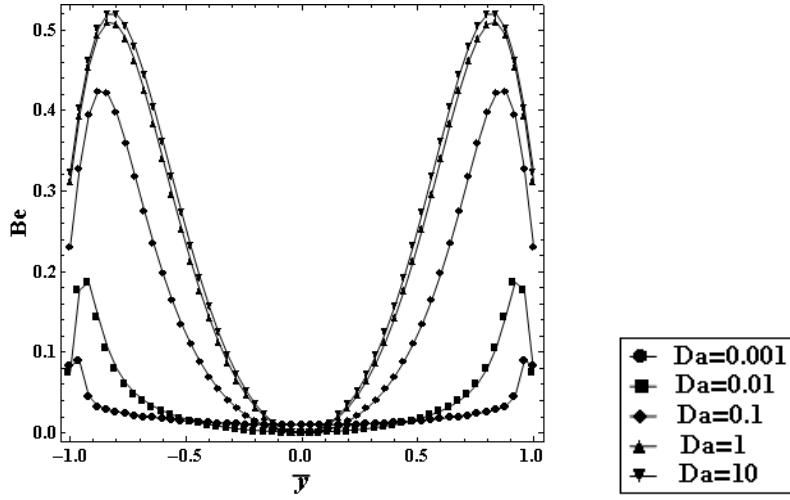


Figure 3.55 : Bejan number for different Da at $\bar{x} = 0.2$, $Pe = 100$, $Br\Omega^{-1} = 0.1$, $Ha = 3$

With the increasing Ha the dominance of heat transfer entropy generation decreases until $Ha = 0$ where there is no contribution of the magnetic effect to the irreversibility generated in the channel.

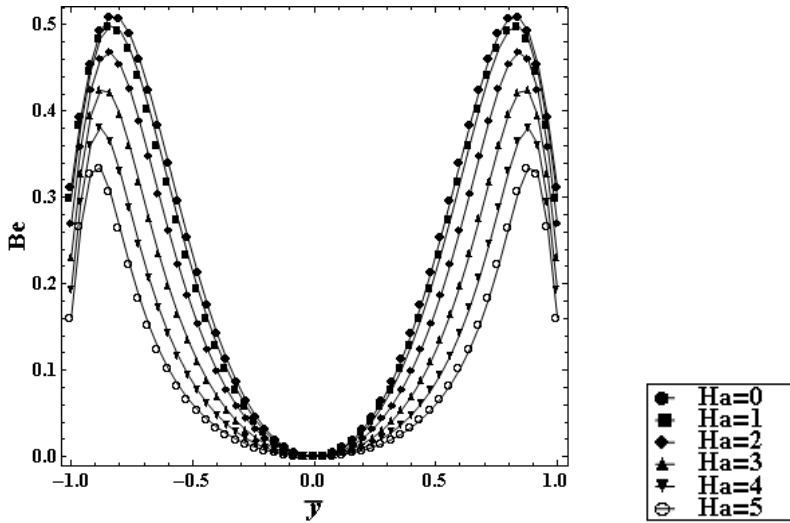


Figure 3.56 : Bejan number for different Ha at $\bar{x} = 0.2$, $Pe = 100$, $Br\Omega^{-1} = 0.1$, $Da = 0.1$

The contribution of each entropy generation mechanisms is investigated and shown in Fig. 3.57. While the entropy generation due to the porous effect, N_p , and magnetic effect, N_m , increases, the entropy generation due to the heat transfer irreversibility, N_h , and entropy generation due to the fluid friction, N_f , irreversibility decrease towards the centreline of the channel. Because of the fact that

the entropy generation due to the porous effect is proportional to the square of the velocity as seen in (2.97).

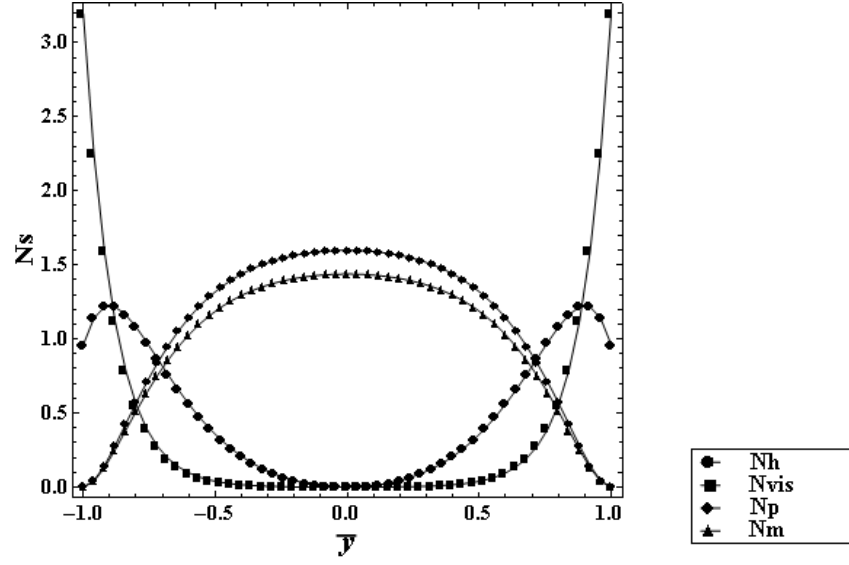


Figure 3.57 : Parts of entropy generation at $\bar{x} = 0.2$, $Pe = 100$, $Br\Omega^{-1} = 0.1$, $Da = 0.1$, $Ha = 3$

The effect of viscous dissipation on the temperature field is shown in Fig. 3.58. There is a difference between the solutions with and without viscous dissipation effect.

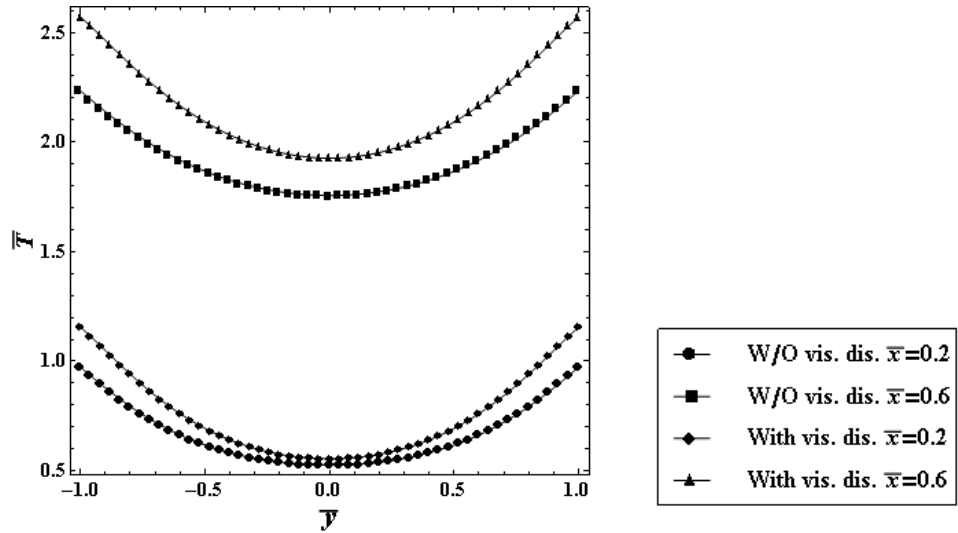


Figure 3.58 : Effect of viscous dissipation on temperature profiles at $Pe = 100$, $Br = 0.1$, $Da = 0.1$, $Ha = 3$

The effect of viscous dissipation on the entropy generation number at different \bar{x} stations where $Pe = 100$, $Br = 0.1$, $Da = 0.1$ is shown in Fig. 3.59. The magnitude of

entropy generation is higher for the case including viscous dissipation. Both Fig. 3.58 and 3.59 shows the fact that the viscous dissipation term in energy equation leads to a great difference.

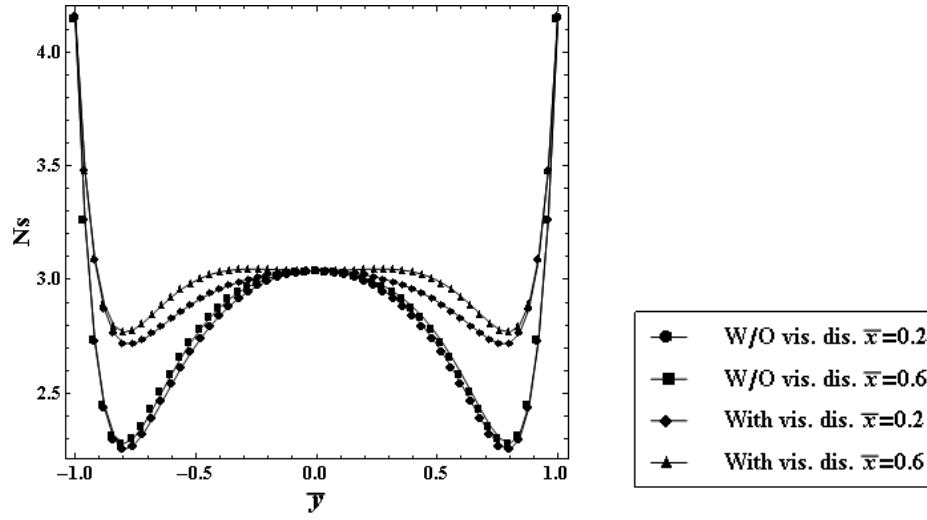


Figure 3.59 : Effect of viscous dissipation on entropy generation at $Pe = 100$, $Br\Omega^{-1} = 0.1$, $Da = 0.1$, $Ha = 3$

4. CONCLUSION AND RECOMENDATIONS

In this study, temperature and flow field are investigated analytical-numerical means for an inclined channel which contains porous medium and magnetic effects, for both Dirichlet and Neumann problems and both together and separately. The flow equation of Newtonian fluid is derived analytically into the channel having heated walls. The governing equations which are related to flow and thermal fields are reduced to dimensionless form by using dimensionless parameters. While the reduced equation for flow field is solved analytically and the reduced equation for thermal field is solved by using FDM. Graphical results for various parametric conditions were comparatively presented and discussed. It was found that the heat and mass transfer mechanisms depend strongly on the characteristic parameters; such as Darcy number (Da), Brinkman number (Br), Hartmann number (Ha), dimensionless axial distance (\bar{x}), dimensionless normal distance (\bar{y}), and flow characteristics.

Additionally, in order to investigate entropy mechanisms for such a geometry and such boundary conditions, the equation of entropy generation, including viscous effects is derived. Then, entropy equation number and Bejan number are plotted for different values of the group parameter ($Br\Omega^{-1}$), Darcy number, Peclet number (Pe) and Hartmann number for different dimensionless axial distances.

Such a physical system including viscous dissipation, porosity and magnetic effects has never been studied before in open literature, to the best of the authors' knowledge. The previous studies, in point of entropy generation view, were either inclined channel with fully clear fluid, either vertical or horizontal channel filled with fully porous zone or magnetic effects without a porous medium. But in this study, it is the first time the entropy generation in an inclined channel filled porous medium with magnetic effects is investigated.

Another importance of this study with which differs from similar studies carried out before is the account of viscous dissipation effect. Therefore, inclusion of this effect

in energy equation and entropy generation calculation results in a deviation from the results calculated without having viscous dissipations. These results are graphically presented in Figs. 3.58 and 3.59. Surely, the correct Second-Low based efficiency calculation of such fluidic system can only be done by inclusion of dissipation effects. This study might encourage the people in this field to consider viscous effects for far more realistic calculations.

REFERENCES

- [1] **Makinde, O. D.**, 2006. Irreversibility analysis for gravity driven non-Newtonian liquid film along an inclined isothermal plate, *Phys. Scr.*, 74 , 642-645.
- [2] **Bejan, A.**, 1980. Second law analysis in heat transfer, *Energy*, 5(8-9), 721-732.
- [3] **Saouli, S., Aiboud-Saouli S.**, 2004. Second law analysis of laminar flow in a channel filled with saturated porous media, *Int. Comm. Heat Mass Transfer*, 31(6), 879-886.
- [4] **Makinde, O. D., Gbolagade, A. W.**, 2005. Irreversibility analysis for gravity driven non-Newtonian liquid film along an inclined isothermal plate, *General Physics, Rom. Journ. Phys.*, 50, 923–930.
- [5] **Havzali, M., Arikoglu, A., Komurgoz, G., Keser, H. I., Ozkol, I.**, 2008. Analytical–numerical analysis of entropy generation for gravity-driven inclined channel flow with initial transition and entrance effects, *Phys. Scr.*, 78(4) , 045401(7).
- [6] **Whitaker, S.**, 1977. Simultaneous heat, mass, and momentum transfer in porous media: A theory of drying, *Advances in Heat Transfer*, Academic Press, New York.
- [7] **Boberg, T.**, 1988. Thermal methods of oil recovery, Wiley, New York, 1988.
- [8] **Cheng, P.**, 1978. Heat transfer in geothermal systems, In: Hartnett JP, Irvine JF Jr. (eds) *Advances in Heat Transfer*, Academic Press, New York.
- [9] **Baytas, A. C.**, 2000. Entropy generation for natural convection in an inclined porous cavity, *Int. J. Heat Mass Transfer*, 43 , 2089-2099.
- [10] **Mahmud, S., Fraser, R. A.**, 2004. Flow and Heat Transfer Inside Porous Stack: Steady State Problem, *Int. Comm. Heat Mass Transfer*, 31(7), 951-962.
- [11] **Makinde, O. D., Osalusi, E.**, 2005. Second Law Analysis of Laminar Flow In A Channel Filled with Saturated Porous Media, *Entropy*, 7, 48-160.
- [12] **Alkam, M. K., Al-Nimr, M. A., Hamdan, M. O.**, 2002. On forced convection in channels partially filled with porous substrates, *Heat and Mass Transfer*, 38, 337-342.
- [13] **Nield, D. A., Bejan, A.**, 1992. Convection in Porous Media, *Springer*, New York.
- [14] **Al-Nimr, M. A., Haddad, O. M.**, 1999. Fully developed free convection in open-ended vertical channels partially filled with porous material, *J. Porous Media*, 2, 179-191.
- [15] **Shokouhmand, H., Jam, F., Salimpour, M.R.**, 2009. Simulation of Laminar Flow and Convective Heat Transfer in Conduits Filled with Porous Media Using Lattice Boltzmann Method, *International Communications in Heat and Mass Transfer*, 36, 378-384.
- [16] **Paul, T., Singh, A. K.**, 1998. Natural Convection Between Coaxial Vertical Cylinders Partially Filled with a Porous Material, *Forschung im Ingenieurwesen*, 64, 157-162.

- [17] **Vasseur, P., Satish, M. G., Robillard, L.,** 1987. Natural convection in a thin, inclined porous layer exposed to a constant heat flux, *Int. J. Heat Mass Transfer*, 30, 2097-2113.
- [18] **Sen, M., Vasseur, P., Robillard, L.,** 1987. Multiple steady states for unicellular natural convection in an inclined porous layer, *Int. J. Heat Mass Transfer*, 30, 2097-2113.
- [19] **Aydin, O., Unal, A., Ayhan, T.,** 1999. A numerical study on buoyancy-driven flow in an inclined square enclosure heated and cooled on adjacent walls, *Numerical Heat Trans., Part A*, 44, 355-373.
- [20] **Mahmud, S., Fraser, R. A.,** 2004. Entropy-energy analysis of porous stack: steady state conjugate problem, *International Journal of Energy*, 1(3), 385-398.
- [21] **Mahmud, S., Fraser, R. A.,** 2004. The second law analysis in fundamental convective heat transfer problems, *International Journal of Thermal Sciences*, 42(1), 177-186.
- [22] **Abu-Hijleh, B. A.,** 2002. Entropy generation due to cross-flow heat transfer from a cylinder covered with an orthotropic porous layer, *Heat Mass Transfer*, 39(2), 27-40.
- [23] **Baytas, A. C.,** 2004. Entropy generation for free and forced convection in a porous cavity and a porous channel in: D.B. Ingham, et. al, (eds.), *Emerging Technology and Techniques in Porous Media*, Kluwer Academic Publishers, pp. 259-270.
- [24] **Hooman, K., Ejlali, A.** 2007. Entropy generation for forced convection in a porous saturated circular tube with uniform wall temperature, *International Communications in Heat and Mass Transfer*, 34, 408-419.
- [25] **Mahmud, S., Fraser, R. A.,** 2005. Flow, thermal, and entropy generation characteristics inside a porous channel with viscous dissipation, *International Journal of Sciences*, 44, 21-32.
- [26] **Makinde, O. D. and Osalusi, E.,** Second law analysis of laminar flow in a channel filled with saturated porous media, *Entropy*, 7(2), 148-160.
- [27] **Tasnim, S. H., Shohel, M., Mamun, M. A. H.,** 2002. Entropy generation in a porous channel with hydromagnetic effect, *Energy*, 2, 300-308.
- [28] **Mahmud, S., Fraser, R. A.,** 2004. Magnetohydrodynamic free convection and entropy generation in a square porous cavity, *Int. J. Heat Mass Transfer*, 47, 3245-3256.
- [29] **Mahmud, S., Fraser, R. A.,** 2003. Mixed convection-radiation interaction in a vertical porous channel: Entropy generation, *Energy*, 28 1557-1577.
- [30] **Url-1** <<http://scienceworld.wolfram.com/physics/PecletNumber.html>>, accessed at 17.10.2009
- [31] **Url-2** <http://en.wikipedia.org/wiki/Brinkman_number>, accessed at 17.10.2009
- [32] **Url-3** <http://en.wikipedia.org/wiki/Hartmann_number>, accessed at 17.10.2009
- [33] **Aiboud-Saouli, S., Settou N., Saouli, S., Meza, N.,** 2007. Second-law analysis of laminar fluid flow in a heated channel with hydromagnetic and viscous dissipation effects, *Applied energy*, 84, 279-289.
- [34] **White, Frank M.,** 2001. Fluid Mechanics. 4th ed. NewYork: McGraw-Hill.
- [35] **Papanastasiou, Tasos C., Georgiou, Georgios C., Alexnadrou, Andreas N.,** 1999. Viscous fluid flow. New York: CRC Press.

- [36] **K. Hooman, F. Hooman, S. R. Mohebpour**, 2008. Entropy generation for forced convection in a porous channel with isoflux or isothermal walls, *Int. J. Exergy*, 5(1), 78-96.
- [37] **Lienhard IV, John H., Lienhard V, John H.**, 2004. A heat transfer textbook, Cambridge: Philogiston Press.
- [38] **Bejan, A.**, 1996. Entropy generation minimization, New York: CRC Press.
- [39] **Gebhart, Benjamin**, 1993. Heat conduction and mass diffsion, New York: McGraw-Hill
- [40] **Mahmud, S. and Fraser, R. A.**, 2003. The second law analysis in fundamental convective heat transfer problems, *International Journal of Thermal Sciences*, 42, 177-186.
- [41] **Mahmud, S. and Fraser, R. A.**, 2001. Thermodynamic analysis of flow and heat transfer inside channel with two parallel plates. *Exergy, an International Journal*, 2, 140-146.
- [42] **Polyanin, Andrei D.**, 2002. Handbook of linear partial differential equations for engineers and scientist, New York: Chapman & Hall/CRC.
- [43] **Aiboud-Saouli S., Saouli, S., Settou N., Meza, N.**, 2006. Thermodynamic Analysis of Gravity-driven Liquid Film along an Inclined Heated Plate with Hydromagnetic and Viscous Dissipation Effects, *Entropy*, 8, 188-199.
- [44] **Hoffmann, Klaus A.; Chiang, Steve T.**, 2000. Computational fluid dynamics vol i. 4th ed., Engineering Education System.
- [45] **Arikoglu, A., Komurgoz, G., Ozkol, I.**, 2008. Effect of Slip on the Entropy Generation From a Single Rotating Disk, *ASME Journal of Fluids Engineering*, 130(10).
- [46] **Arikoglu, A., Komurgoz, G., Ozkol, I.**, 2008. Effect of slip on entropy generation in a single rotating disk in MHD flow, *Applied Energy*, 85, 1225–1236.

CURRICULUM VITA



Candidate's full name: Murat Havzalı
Place and date of birth: Amasya / Merzifon 13.12.1982
Permanent Address: havzali@itu.edu.tr
Universities and Colleges attended: Istanbul Technical University

Publications:

- **Havzalı, M.**, Arikoglu, A., Komurgoz, G., Keser, H. I., Ozkol, I., 2008: Analytical–numerical analysis of entropy generation for gravity-driven inclined channel flow with initial transition and entrance effects, *Phys. Scr.*, 78, 045401, (7pp), Istanbul, TURKEY.
- **Havzalı, M.**, Komurgoz, G., Arikoglu, A., Keser, H. I., Ozkol, I., 2009: Second law analysis of porous medium inclined channel including dissipation effects, *Phys. Scr.* (Being reviewed), Istanbul, TURKEY.